Challenge Journal of

CONCRETE RESEARCH LETTERS

Vol.14 No.3 (2023)

absorption aerated concrete artificial neural network compressive strength concrete corrosion cracking curing ductility durability energy absorption ferrocement flexural strength fly ash fracture mechanics mechanical properties mortar nanoparticle reinforced concrete self- compacting concrete steam curing strengthening superplasticizer tensile strength workability waste disposal water absorption

ISSN 2548-0928

TULPAR ACADEMIC PUBLISHING

Challenge Journal of Concrete Research Letters

EDITOR IN CHIEF

Prof. Dr. Mohamed Abdelkader ISMAIL	*Miami College of Henan University, China*

EDITORIAL BOARD

Prof. Dr. Ashraf Ragab MOHAMED	*Alexandria University, Egypt*
Prof. Dr. Ayman NASSIF	*University of Portsmouth, United Kingdom*
Prof. Dr. Gamal Elsayed ABDELAZIZ	*Benha University, Egypt*
Prof. Dr. Hamidah Mohd SAMAN	*Universiti Teknologi Mara, Malaysia*
Prof. Dr. Han Seung LEE	*Hanyang University, Republic of Korea*
Prof. Dr. Zubair AHMED	*Mehran University, Pakistan*
Prof. Dr. Jiwei CAI	*Henan University, China*
Prof. Dr. Jahangir MIRZA	*Hydro-Québec Research Institute, Canada*
Prof. Dr Ahmet Ferhat BİNGÖL	*Atatürk University, Türkiye*
Assoc. Prof. Dr. Meral OLTULU	*Atatürk University, Türkiye*
Assoc. Prof. Dr. Saleh Omar BAMAGA	*University of Bisha, Saudi Arabia*
Assoc. Prof. Dr. Mohammed Seddik MEDDAH	*Sultan Qaboos University, Oman*
Assoc. Prof. Dr. Brabha NAGARATNAM	*Northumbria University, United Kingdom*
Dr. Aamer Rafique BHUTTA	*Aramco, Saudi Arabia*
Dr. Khairunisa MUTHUSAMY	*Universiti Malaysia Pahang, Malaysia*
Dr. Mahmoud SAYED AHMED	*Ryerson University, Canada*
Dr. Jitendra Kumar SINGH	*Hanyang University, Republic of Korea*
Dr. Türkay KOTAN	*Erzurum Technical University, Türkiye*
Dr. Ali KEYVANFAR	*Kennesaw State University, United States*
Dr. Arezou SHAFAGHAT	*Kennesaw State University, United States*

E-mail: *cjcrl@challengejournal.com*

Web page: *cjcrl.challengejournal.com*

TULPAR Academic Publishing
www.tulparpublishing.com

Challenge Journal of Concrete Research Letters

CONTENTS

Research Articles

Evaluation of the lightweight foamed concrete characteristics **59–68**
Zeinab A. Etman, Samar A. Rokbah

Performance of light weight ferrocement composite walls **69–88**
Yousry B. I. Shaheen, Zeinab A. Etman, Doha E. A. Kandil

Mechanical, durability and solar reflectance properties of colored self–compacting concrete **89–95**
Sadık Alper Yıldızel

TULPAR ACADEMIC PUBLISHING

Challenge Journal of Concrete Research Letters

Research Article

Evaluation of the lightweight foamed concrete characteristics

Zeinab A. Etman [a,b], Samar A. Rokbah [b,*]

[a] Department of Civil Engineering, Menoufia University, Shebin ElKoum, Menofia, Egypt
[b] Department of Civil Engineering, Higher Institute of Engineering and Technology, Menofia, Egypt

ABSTRACT

The purpose of this paper is to assess the properties of light weight foamed concrete. In this research, two phases are investigated. The first stage explored the characteristics of fresh and hardened foamed concrete using a foaming agent. The following parameters were employed in this study: foaming agent used as a volume of concrete mix by 10, 20, and 40%, fly ash used as a replacement of cement content by 10, 25, and 50%, and polypropylene fiber used with varied volume fractions of 0.5, 0.75, and 1.0%. Slump values are applied to evaluate the fresh properties. To evaluate the hardened concrete, the dry density and compressive strength at 7 and 28 days are computed. Furthermore, the 28-day tensile splitting strength and flexural strength are studied. The effect of a high temperature was evaluated. The second stage investigated the effects of polypropylene fiber on both fresh and hardened concrete. It was observed that foaming agents improve fresh characteristics while decreasing compressive strengths and dry density. Furthermore, utilizing fly ash improves the characteristics of both fresh and hardened foamed concrete. The fiber reduces the fresh characteristics while enhancing the toughened properties. Because of its low density, foamed concrete is being used for structural applications because of this study. Such as those utilized for thermal insulation, acoustic impedance, and fire breaks. Also used to create road foundations for roads built on soft soil.

ARTICLE INFO

Article history:
Received 8 February 2023
Revised 21 March 2023
Accepted 9 April 2023

Keywords:
Lightweight concrete
Foamed concrete
Foaming agent
Fly ash

1. Introduction

Foam concrete is a form of cement mortar containing cement, water, and foam brought using an appropriate foaming agent. Other research's describing this material as lightweight cell concrete, low-density foam concrete, or cell lightweight concrete, and many others. In applications, it offers pleasant answers to cope with various challenges and troubles faced in construction activities Fu et al. (2020). Mainly for lowering the dead load of structures and for heat preservation, damping, sound insulation, and pore filling. The researchers found that the chemical foaming approach is more suitable for ultra-lightweight FC than mechanical foaming. Shi et al. (2019) Used ultra-lightweight expanded polystyrene foamed concrete (EFC), and its thermal insulation property was measured. It was noticed EFC thermal conductivity declines as the temperature exceeds. In addition, the precise volume of EPS particles can't only reduce the EFC thermal conductivity however also decrease the influence of temperature at the thermal conductivity. FC can be produced through addition of pre-foam into mortar to produce FC without filler or FC with filler, consisting of fly ash, quarry dust.

Habsya et al. (2018) studied the influence of foaming agent and fly ash content material at the density, thermal conductivity, compressive strength, and water absorption of lightweight Foamed Concrete (LFC). The results indicated that the increasing of foam content decreases density, thermal conductivity, and compressive strength of LFC and increases water absorption. On the other hand, the increasing of FA content decreases water absorption, but it will increase density, thermal conductivity, and compressive energy.

Kearsley and Wainwright (2001) studied the porosity and permeability of replacing a large content of cement

* *Corresponding author*. Tel.: +20-102-561-8461 ; Fax: +20-048-257-4279 ; E-mail address: samar.roanas@gmail.com (S. A. Rokbah)
ISSN: 2548-0928 / DOI: https://doi.org/10.20528/cjcrl.2023.03.001

up to 75% with both classified and unclassified fly ash. Porosity was mainly dependent on the dry density now not on ash content or kind, which became more for foamed concrete. The permeability increased with growing porosity and ash content material.

Gopalakrishnan et al. (2020) investigated the impact of fly ash with the aid of partially changing in cement as much as 50% and replacing river sand by quarry dust as much as 50% for diverse mixes. It has been concluded that the changing partially 30% of first-rate sand b and quarry dust mixture produced higher first-class effects in par with the conventional foam concrete.

Kanagalakshmi et al. (2015) studied the effect of quarry dirt substitute (0-50%) with sand on compressive strength of foamed concrete. The results indicated the compressive strength of foam concrete product of quarry dust extra than the control foam concrete by 43%. So that, it was proposed that burnt clay bricks can be effectively replaced with foam concrete blocks. Many types of fibers have been used to observe the properties of foamed concrete.

Regarding natural fibers and synthetic such as, polypropylene fiber, steel; Raupit et al. (2017) discovered that the addition of polypropylene fiber to the lightweight foamed concrete does affect the tensile strength of the foamed concrete. However, Atoyebi et al. (2018) studied the steel fiber content material in specimens increases the splitting tensile strength decreases. While Hazlin et al. (2017) concluded that foamed concrete added by Polypropylene fibers gave better performance in tensile strength in comparison to foamed concrete without Polypropylene fibers. This study shows the mechanical properties of foamed concrete, and the influence of elevated temperatures on it.

2. Significance of the Research

With urban growth, there is a need to identify and produce sustainable materials that aid in long-term development. The necessity of the day is for a lightweight material with a low self-weight that uses by-products or wastes. Because of its light weight, foam concrete is becoming increasingly common. Therefore, the aims of this paper are:

- To investigate the influence of different percentages fly ash on foam concrete.
- Investigate the impact of different volume fraction of polypropylene fibers on foam concrete.
- To investigate the effect of high temperature of the properties of foam concrete.

3. Experimental Program

All tests in this paper were conducted in the Civil Engineering Department's Quality Control and Strength of Testing Materials Laboratory at the Higher Institute of Engineering and Technology, Menoufia, Egypt. The following sections detailed the materials used, as well as how to prepare, cast, cure, and test testing specimens.

3.1. Materials

3.1.1. Cement

The Lafarge Cement Factory manufactured Portland cement (CEM I 42.5 N) with specific gravity 3.15 in accordance with (E.S.S.47651-1/2013) and (E.P.C 203/2018).

3.1.2. Sand

Natural siliceous sand that satisfies the Egyptian standard specifications (E.S.S.1109/2008). It is practically impurity-free, with a specific gravity of 2.6 t/m^3 and a fineness modulus of 2.61.

3.1.3. Fly ash

Class (F) fly ash with a specific gravity of 2.3 was utilized to fulfill the requirements of (ASTM C618).

3.1.4. Water

Water per binder (fly ash+ cement) ratio (w/b) was 0.30. Tap water was used for mixing the concrete conformed to the requirements of (E.P.C 203/2018).

3.1.5. Foaming agent

Foaming agent type EUCO from Swiss Chemistry Factory is chloride free. It was used to produce lightweight concrete by entraining a controlled amount of air bubbles to concrete mix. Table 1 indicates the properties of the foaming agent used throughout this investigation.

3.1.6. Fiber

Polypropylene fibers were used (Table 2, Fig. 1). The fibers accounted of the total mix volume was utilized to fulfill the requirements of (ASTM C1116).

Table 1. Properties of the foaming agent.

Appearance	liquid
Color	transparent
Specific gravity	1,01
Viscosity	6,5 MPA
Chloride content	nil
Compatibility with cement	all types of Portland cement
Shelf life	up to 2 years
Surface tension ASTM C 233	41,9 N/cm^2

Table 2. Properties of the polypropylene fibers.

Length range (mm)	(12-20)
Average diameter (μm)	20
Aspect ratio (L/d)	800
Tensile Strength (MPa)	550-600
Fiber elongation (%)	14-25%
Specific gravity (kg/m^3)	0.9
Melting point	160° C
Burning point	590° C

Fig. 1. Polypropylene fibers used in this research.

3.2. Methodology

At the beginning, the start points of choosing the proportions of foamed concrete mixes was conducted firstly based on previous research as reported by Kanagalakshmi et al. (2015), Roslan et al. (2013), and Reddy et al. (2017). The methodology for producing foam concrete (Fig. 2, Table 3) with the required characteristics varies substantially. The concrete was mixed in the following method to achieve the target density of 1500-1800 kg/m^3.

To create the foam, the foam agent was diluted 1: 30 with water weight and blended with a mixer at 500 cycles per minute for 10 minutes. On the other hand, dry materials such as cement, sand, and fly ash were mixed thoroughly then added the water to dry materials. Next, the prepared foam added to the mortar and blended the mixing uniformly. The foamed concrete was ready for pouring once the foam had been thoroughly integrated. The foamed concrete was manually placed. After 24 hours, the foamed concrete has achieved green strength and must be left to air cure before water curing can begin. This approach was employed in Reddy et al. (2017).

The conducted experimental program was divided into two stages. The first stage was performed to study the effect of using foaming agent and fly ash on the fresh and hardened concrete properties. Based on the test results of the previous stage, the best-recorded values were used in the second stage. The second stage was conducted to study the effect of using polypropylene fiber with different volume fraction in foamed concrete on the fresh and hardened concrete properties.

a) Mix of the dry components b) Foam generated c) The mix after adding foaming agent

Fig. 2. Procedures of foamed concrete mixture.

Table 3. Constituents of concrete mixes (kg/m^3).

	Sample Type	Mix no	Cement	Sand	Water	Fly ash	Polypropylene (fiber)	Foaming agent (% of mixture volume)
Stage 1	0% F	C1	746.27	1119.36	335.80	0.00	0.00	0.0
	10% F	C2	671.64	1007.46	201.49	0.00		100
	20% F	C3	597.01	895.58	179.10	0.00		200
	40% F	C4	447.76	671.64	134.33	0.00		400
	10% FA + 10% F	M1	604.476	1007.46	201.49	67.16		100
	10% FA + 20% F	M2	537.309	895.58	179.10	59.70		200
	10% FA + 40% F	M3	402.984	671.64	134.33	44.78		400
	25% FA + 10% F	M4	503.73	1007.46	201.49	167.91		100
	25% FA + 20% F	M5	447.76	895.58	179.10	149.25		200
	25% FA + 40% F	M6	335.82	671.64	134.33	111.94		400
	50% FA + 10% F	M7	335.82	1007.46	201.49	335.82		100
	50% FA + 20% F	M8	298.505	895.58	179.10	298.50		200
	50% FA + 40% F	M9	223.88	671.64	134.33	223.88		400
Stage 2	0.5% PP + 25% FA + 10% F	M10	504.73	1009.5	201.89	168.25	4.50	100
	0.75% PP + 25% FA + 10% F	M11	503.29	1006.58	201.32	167.76	6.75	100
	1.0% PP + 25% FA + 10% F	M12	501.88	1003.75	200.75	167.29	9.00	100

PP: Polypropylene fiber FA: Fly ash F: Foaming agent

3.3. Testing method

3.3.1. Slump test

Inverted slump test was conducted to determine the consistency of foamed concrete. This test was conducted according to ASTM C143M-03.

3.3.2. Dry density

The dry density test was determined from the dried weight (105 °C for 24 hrs). Three 50mm cubes were measured in each sample tested. The density defined as the mass of the concrete divide in its volume. The dry density it tested at age (28) days. Also, after the specimens exposed to elevated temperatures densities were calculated.

3.3.3. Compressive strength

Cube specimens of dimensions 100x100x100 mm are prepared for evaluating the compressive strength. According to ASTM C109 the compressive strength test was carried out. A 2000 KN capacity compression testing machine is used. Average compressive strength was obtained based on three cubic specimens.

3.3.4. Splitting tensile strength

Cylindrical concrete specimens, 100 mm in diameter and 300 mm in high, are prepared to evaluate the splitting tensile strength. Indirect tension test (splitting method) is performed to determine the tensile strength of concrete mixes. ASTM C39 was used to conduct the splitting tensile strength. A 2000 KN capacity compression testing machine is used.

3.3.5. Flexural strength

This test method evaluates the flexural strength obtained by a testing simply supported beam (prism) under four - point loading at universal testing machine according to ASTM C78.

3.3.6. Elevated temperature and testing methodology

Throughout this investigation, three specimens representing the same ingredient are utilized for each test, and the average values are presented.

The compressive strength of an unheated control specimen is measured after 28 days; the other specimens are heated to target temperature in an electric furnace with a capacity of 1200 °C, as shown in Fig. 3, at a heating rate of 10 °C/min. There are two target temperatures: 200 °C and 400 °C. For 1.5 hours, the specimens are held at each temperature. The specimens are allowed to cool for 24 hours at laboratory room temperature after being subjected to the required temperature before being evaluated to assess residual strength after 1 day. On a dry surface, the specimens are assessed. For each test data point, three data points were gathered.

Fig. 3. Electric furnace used in this research.

4. Results and Discussions

The characteristics of Foamed Concrete were studied using various parameters. The outcomes of the experimental program are described in detail in the following sections.

4.1. Consistency of the foamed concrete

Fig. 4 shows the results of slump tests performed using foaming agents. The figure also demonstrates the relation between the slump and the amount of foaming agent used (as a ratio of volume concrete mixture). The results demonstrated that as the foamy agent dose increased, the slump values increased when compared to the control mix with 0.0% foaming agent. The workability of foaming agent and fly ash mixtures increased as the foaming agent increased. For example, for 10%, 20%, and 40% foaming agent, the slump results were 100, 140, and 200 mm, respectively.

Furthermore, it demonstrates that when the fly ash concentration increases, the workability of concrete decreases, which may be ascribed to the higher particle surface of fine fly ash compared to cement as described by Othman et al. (2021).

Fig. 5 shows the results of slump tests conducted using polypropylene fibers. The figure also illustrates the relationship between slump and fiber percentage (volume fraction). When compared to a control mix of 25% fly ash and 10% foaming agent, the slump values reduced as fiber increased. Slump findings demonstrate that fibers with 0.5, 0.75, and 1.0% V_f have 115, 80, and 30 mm, respectively. The decrease in slump because of polypropylene fiber tend to absorb water which lead to, the weakening of resistance between the structures of the mix and contraction of the free water amount, that explains the decrease of slump diameter consistently to the presence of polypropylene fiber Mydin et al. (2023).

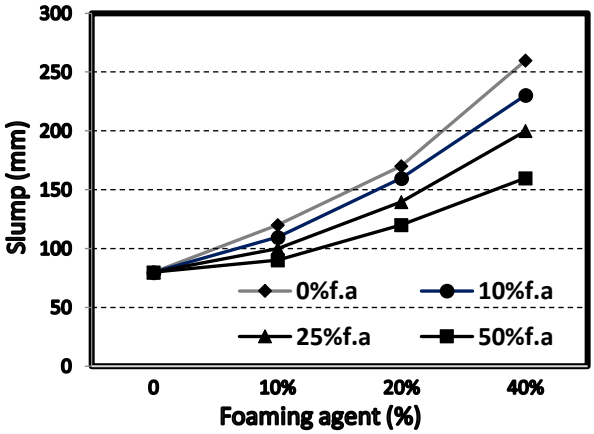

Fig. 4. Slump values of foamed concrete due to foaming agent.

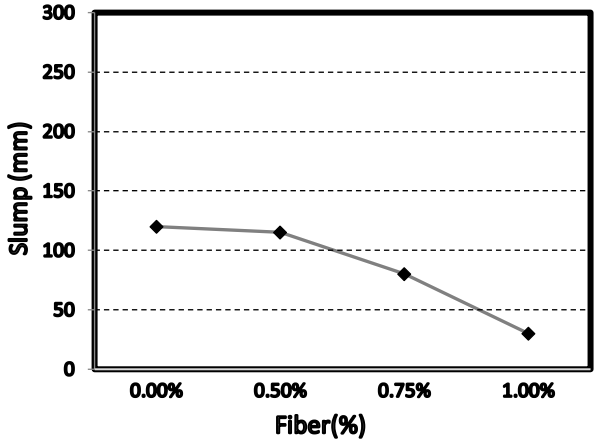

Fig. 5. Slump values of foamed concrete due to polypropylene fibers.

4.2. Dry density of the foamed concrete

The dry density has been investigated, as seen in Fig. 6. The density of the mixes with foaming agent was somewhat greater than the density of the fly ash mixtures. The result indicated that for mixes with foaming agent only, the densities declined when compared to the control mix with 100% cement. The lowest dry density was 1600 kg/m^3 for the mix with 40% foaming agent.

The similar pattern was seen in mixes with fly ash replacement with cement. The lowest dry density was 1565 kg/m^3 for mix-9, followed by 1570 kg/m^3 for mix-6, and 1585 kg/m^3 for mix-3. Because cement has a higher specific gravity than fly ash, the density of mixtures including fly ash is lower. The density of foamed concrete, according to Nambiar and Ramamurthy (2006), is dependent on the filler type, such as fly ash, which has a low specific gravity compared to fine sand. Similarly it was reported by Gencel et al. (2022) and Krishna et al. (2021) the dry density decreased as the volume of foam and the weight of fly ash increased.

The effect of fiber on dry density has been explored in Fig. 7. The density of the mix with 0.50% V_f of fiber was rather greater than the density of the control mixes without fiber (25% fly ash + 10% foam). Moreover, when the fiber content increased, the dry density reduced. The lowest dry density for 1.0% V_f fiber was 1748 kg/m^3, followed by 1750 kg/m^3 for 0.75% V_f, and 1760 kg/m^3 for 0.5% V_f.

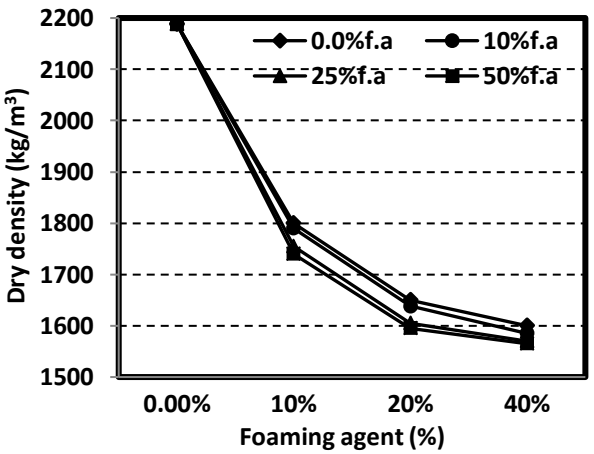

Fig. 6. Relation between foaming agent and dry density.

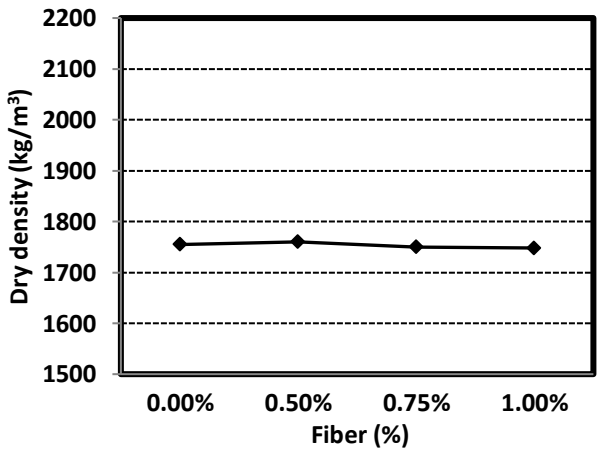

Fig. 7. Relation between fiber and dry density.

4.3. Compressive strength of the foamed concrete

Figs. 8-11 show the findings of the mechanical properties evaluated. Figs. 8 and 9 illustrate the relationship between foaming agent dose and compressive strength values for mortars with 0.0, 10, 25, and 50% fly ash replacement with cement after 7 and 28 days. The figures revealed that when the foaming agent was increased, the compressive strength decreased compared to the control mix for the mix without fly ash. However, when comparing the fly ash-containing mixtures, at all the foaming agent doses were more than the control mixture. Gopalakrishnan et al. (2020) achieved comparable findings. At test ages of 7 and 28 days, the optimum compressive strength for mix with a foaming agent only achieved at 10% foaming agent which was less than the control mix by 36%. Consequently, when the fly ash content increased, the compressive strength increased. The compressive strength, increased up to 25 % fly ash then decreased compared to control mix. At 7 and 28 days, the ultimate compressive strength of mixes containing 25, 10, and 50% fly ash was 45, 34.5, and 29% greater than

the control mix. The increase in compressive strength owing to CSH production is connected to the constant reduction of pore size and the reduction of calcium hydroxide (CH) crystals, both of which have a damaging effect on the binding between the cement paste and aggregates.

Figs. 10 and 11 indicate the relationship between fiber % and compressive strength after 7 and 28 days, respectively. The analysis indicated that as the fiber density increased, the compressive strength reduced in comparison to the control mix. For 0.5, 0.75, and 1.0% V_f, the reduction was 20.67, 32.5, and 42.17%, respectively. The decrease in compressive strength was due to the addition of polypropylene fiber, especially at 0.75 and 1.00% V_f. The addition of fiber produces additional pores and voids, resulting in a weak connection between pore, void, and matrix as mentioned by Roslan et al. (2013). This is agreed with Falliano et al. (2019) that concluded the effect of fiber on compressive strength can be neglected specifically on dry density lower than 400 kg/m^3. This is because the compressive strength is influenced by the volume of produced air provided by the foam (air/cement ratio), which is not affected to normal-weight concrete but of interest in light weight concrete. Modes of failure under compression loads are presented in Fig. 12.

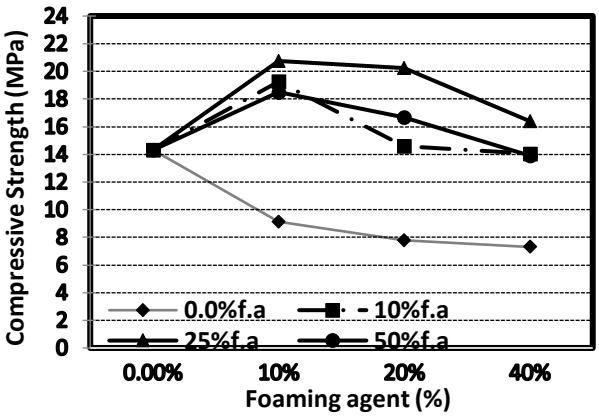

Fig. 8. Compressive strength values at 7 days of foaming concrete due to foaming agent and fly ash.

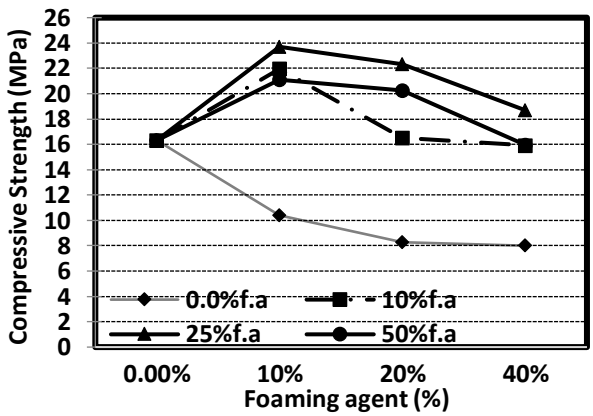

Fig. 9. Compressive strength values at 28 days of foaming concrete due to foaming agent and fly ash.

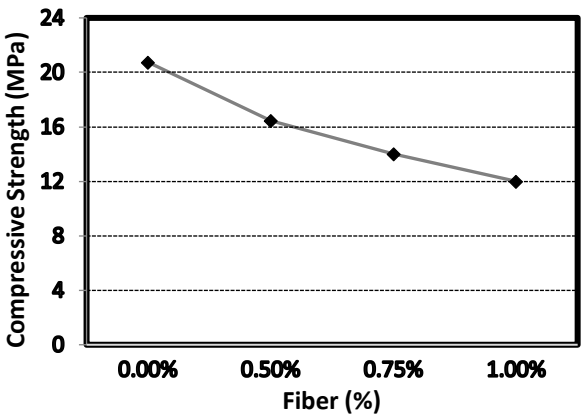

Fig. 10. Compressive strength values at 7 days of foaming concrete due to PP fiber.

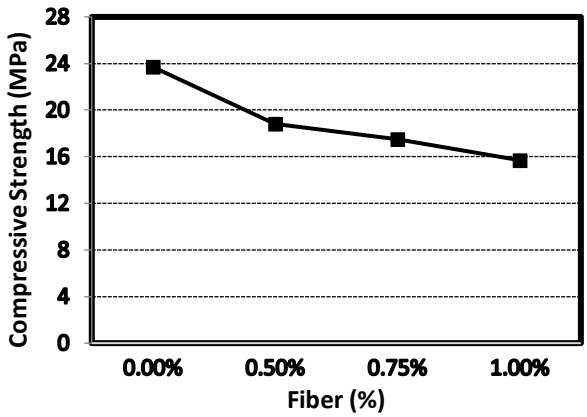

Fig. 11. Compressive strength values at 28 days of foaming concrete due to PP fiber.

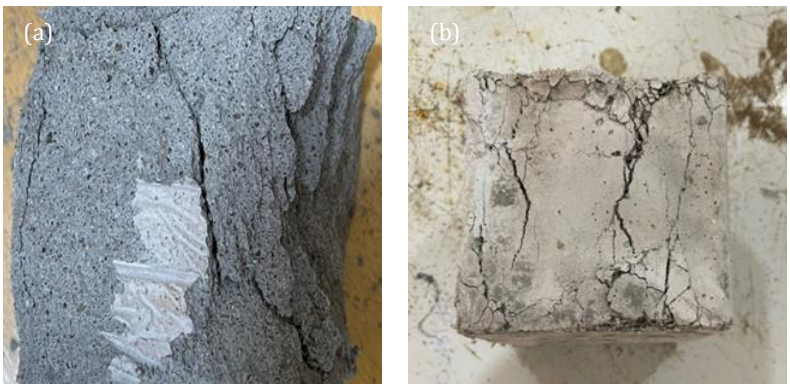

Fig. 12. Modes of failure under compression loads: (a) Normal LFC; (b) LFC with PP fiber.

4.4. Split tensile strength of the foamed concrete

Fig. 13 shows the relationship between the foaming agent dosage and the tensile splitting strength for mortars at 0.0, 10, 25, and 50% fly ash replacement with cement at 28 days. The splitting tensile strength gives the same trend as compressive strength. From Fig. 13, for mix without fly ash as the foaming agent increased the splitting tensile strength decreased compared to control mix. The maximum tensile splitting strength at 28 days obtained at foaming agent dosage equal to 10% of volume mixture.

For the mixes with fly ash the tensile strength increased as the fly increased up to 25 % fly ash then decreased compared to control mix. The maximum tensile strength recorded at 10% foaming agent. For mixes with 10, 25, 50 % fly ash replacement with cement, which, increment by 12.5, 14.4, and 10% respectively compared with control mix. On the other hand, mixes with 25, and 50% fly ash recorded increment by 12.5, and 8.75 % at 20% foaming agent, and increment by 6.25% at 40 % foaming agent compared to control mix. While mixes with 10% fly ash show decrement in strength by 0.0, and 6.25% at 20, and 40 % foaming agent compared to control mix.

The spitting tensile strength of foamed concrete due to fiber is presented in Fig. 14. It can be seen the mixes with fibers improved the tensile strength compared to control mix. The maximum tensile strength recorded is at 0.50% V_f of fiber. The increment by 57, 20, 9% at 0.50, 0.75, and 1.00% V_f of fiber respectively compared to control mix. The increase occurs due to the increasing density and decreasing foam volume Hazlin et al. (2017).

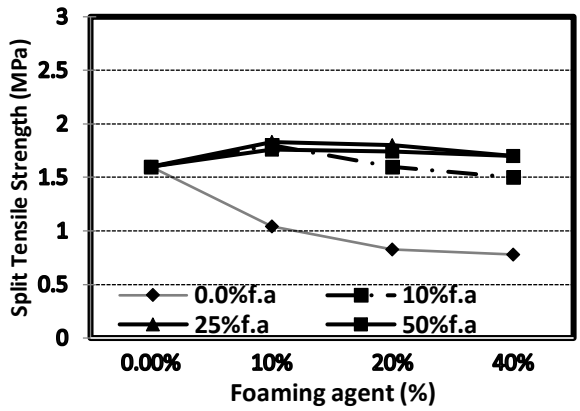

Fig. 13. Splitting tensile strength values at 28 days for foamed concrete due to foaming agent and fly ash.

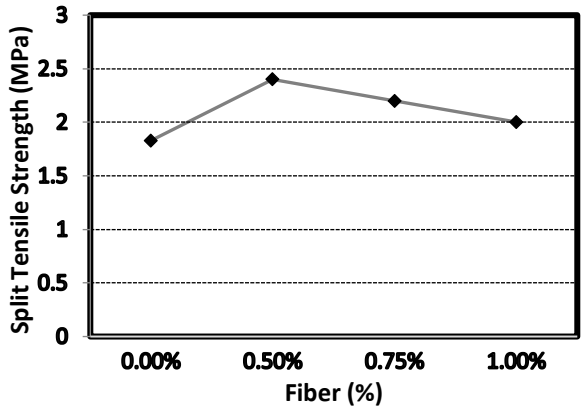

Fig. 14. Splitting tensile strength values at 28 days for foamed concrete due fiber.

4.5. Flexural strength of the foamed concrete

The relationship between the foaming agent dose and the flexural strength for mortars at 0.0, 10, 25, and 50% fly ash replacement with cement at 28 days is shown in Fig. 15. The figure shows that the flexural strength of the mix without fly ash decreased as the foaming agent increased when compared to the control mix. Flexural strength decreased by 37, 49.6, and 49.75% for mixes containing 10, 20, and 40% foaming agent, respectively, as compared to the control mix. Furthermore, for mixes including fly ash, the flexural strength dropped as the foaming agent increased. The greatest flexural strength was observed at 10% foaming agent in mixes with 10, 25, and 50% fly ash substitution with cement.

Fig. 16 displays the flexural strength of foamed concrete owing to fiber. The mixtures with 0.75% and 0.50% V_f of fibers had slightly higher flexural strength than the control mix without fiber. Then it fell to 1.00% V_f of fiber. The increase was 2.1, 3.25, and -3.56% for 0.50, 0.75, and 1.00% V_f of fiber, respectively, as compared to the control mix.

The increasing of fiber increased flexural strength this corresponds to the increasing in density. This is because the solid phase is higher (the porosity is lower) for that higher density for volume size of specimens. So that, the fibers collaborate with cementitious matrix in a more effective manner and contribute to the overall strength more significantly Falliano et al. (2019). It can be drawn that the presence of fiber acts as a reinforcing tissue to bind the matrix of composite material firmly compared to the specimen without any fiber applied in the tensile zone as reported by Roslan et al. (2013) and Serudin et al. (2019). The use of fiber not only reduced the strength of the foamed concrete, but also demonstrated ductile behavior and prevented the specimen from being split into two sections. Fig. 17 represents the mode of failure due to fiber in foamed concrete.

4.6. Effect of elevated temperature on the foamed concrete

Fig. 18 displayed the calculated compressive strength of foamed concrete after 1.5 hours of exposure to 200 and 400 °C due to foaming agent and fly ash. As the exposure temperature increased, the compressive strength of foamed concrete deteriorated. According to Fig. 18 the compressive strength after exposure to 200 and 400°C for the mixes contain (10-40%) foaming agent are lower than that of control mix at the same temperature. From results, the reduction in compressive strength of its original at 200 °C by 27.9, 18.1, 10% and at 400°C by 32.7, 39.8, and 15 % for 10, 20, and 40% foaming agent respectively. This is due to the dehydration of CH into calcium oxide causes the paste to shrink and fracture after being exposed to increased temperatures of 200 °C and higher. As calcium oxide rehydrates, it expands and cracks, causing more disintegration.

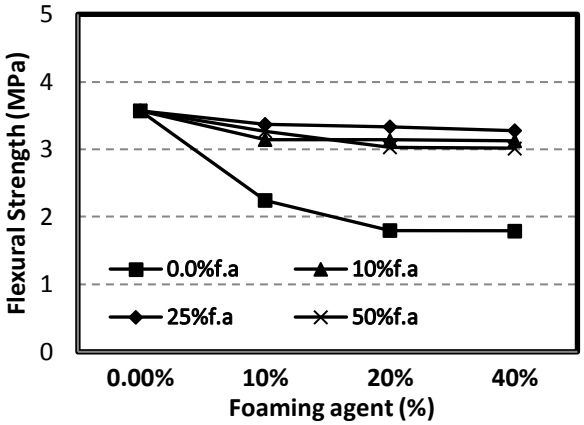

Fig. 15. Flexural strength values at 28 days for foamed concrete due to foaming agent and fly ash.

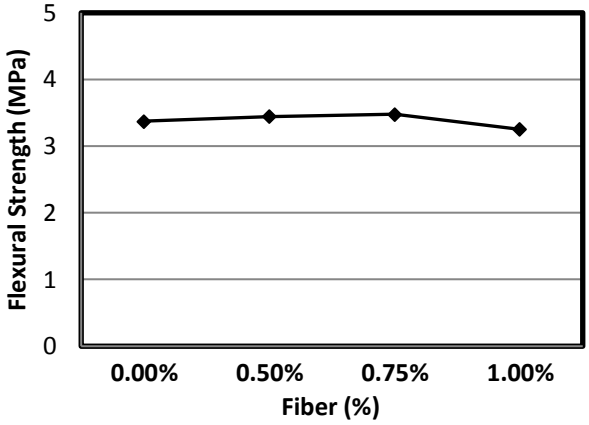

Fig. 16. Flexural strength values at 28 days for foamed concrete due to fibers.

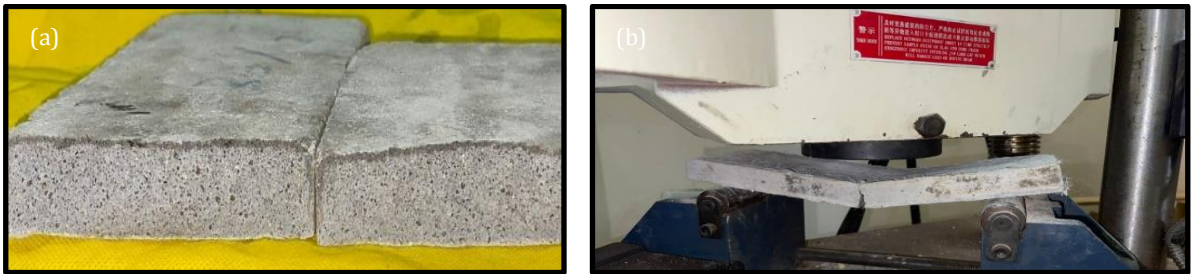

Fig. 17. Modes of failure under flexural load: (a) Normal LFC; (b) LFC with PP fiber.

The compressive strength after exposure to 200 and 400 °C for the mixes contain fly ash replacement with cement by (10, 25, and 50%) are higher than that of control mix at the same temperature. The minimum reduction in compressive strength of its value at 10 % fly ash, while the maximum reduction in compressive strength of its value recorded for mixes with 50% fly ash. The reduction by 20.4, 27.7, and 13.5% for 10, 20, and 40% foaming agent respectively.

Fly ash increases the strengths of concrete against high temperature due to the formation of tobermorite that is a product of lime and FA at high pressure and temperature which is about two to three times stronger than the CSH gel Soleimanzadeh et al. (2013)

Fig. 19 illustrates the compressive strength after exposure to 200 and 400 °C due to fibers. It can be concluded as temperature increased the compressive strength decreased for mixes with fiber compared with control mix with no fiber. The lowest residual compressive strength recorded for mix with 0.75 % V_f fiber followed by 0.5% V_f then 1.0% V_f, when the temperature reached 200 °C and 400 °C. The increase of fiber ratio caused a decrease in the strength after high temperature. This is due to after temperature increased melting of Polypropylene fiber at (160 °C) increases since, the void structure and deterioration of the internal structure causes the strength decreased Kaya and Köksal (2021), and Dawood et al. (2019). While Karahan et al. (2019) reported that the influence of Polypropylene fiber addition in mortar after elevated temperature showed that better behavior at 200 °C and 400 °C for any cooling method. Furthermore, at 600 °C and 800 °C, mortar with polypropylene fiber had behavior like to control mortar.

5. Conclusions

Based on the results and discussion presented in this paper, the following conclusions could be drawn as follow:

- Increasing the foaming agent dosage improved foam concrete workability while increasing the fly ash and fiber dosages decreased workability.
- The use of a foaming agent, fly ash, and fiber reduced the density of the mixes. This would stimulate the use of foamed concrete in projects with low density characteristics.
- It is possible to produce lightweight foamed concrete with densities ranging from 1550 to 1800 kg/m^3.
- Using foaming agent decreased the compressive strength. The optimum value for foaming agent is 10%, where the compressive strength at 28 days and dry density were 10.4 MPa and 1800 kg/m3, respectively.
- Using fly ash for the foamed concrete with 10% foaming agent improved the strength of the mix. The highest compressive strength and dry density were 23.7 MPa and 1755 kg/m^3, respectively at 25% of fly ash as a replacement of cement content as an optimum value.
- Using polypropylene fiber for the foamed concrete with 10% foaming agent and 25% fly ash as a replacement of cement content reduced the compressive strength. The maximum compressive strength and dry density were 18.8 MPa and 1760 kg/m^3 at 0.50% V_f of fiber as an optimum value.
- Using foaming agent dosage decreased the split tensile strength, the optimum tensile strength for foamed concrete was 1.04 MPa at 10% foaming agent as an optimum value. On the other hand, using of the fly ash

and fiber in foamed concrete developed the tensile strength. The optimum tensile strength was 1.83 and 2.4 MPa at 25% fly ash and 0.5% V_f respectively as an optimum value.

- Using foaming agent and fly ash in foamed concrete reduced the flexural strength. While, using fiber developed the flexural strength and mode of failure. The maximum flexural strength was 3.48 MPa at 0.75% V_f as an optimum value.
- In terms of residual strength, the performance of foamed concrete at increased temperatures up to 400 °C was quite efficient. The minimal drop in compressive strength of its original is 40% for mixes including 10% foaming agent, 25% of fly ash as a replacement of cement, and 0.75% volume fraction of polypropylene fiber. This would promote the usage of foamed concrete as an insulating material.
- Foamed concrete is being used for structural applications because of this study. Such as those utilized for thermal insulation, acoustic impedance, and fire breaks. Also used to create road foundations for roads built on soft soil.

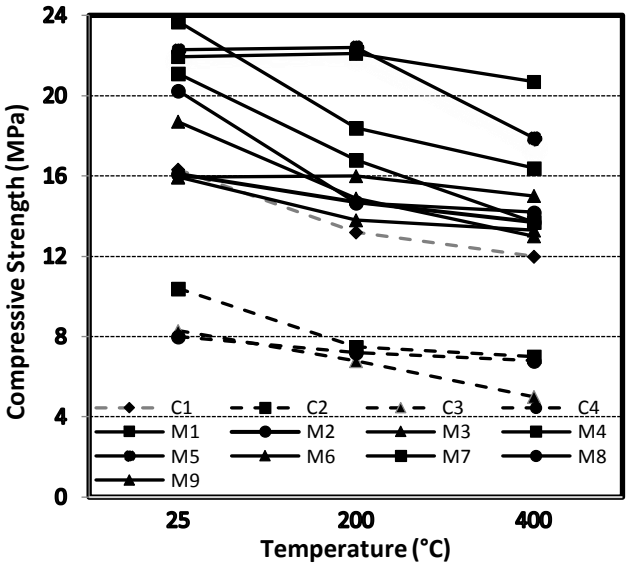

Fig. 18. Compressive strength at elevated temperature due to foaming agent and fly ash.

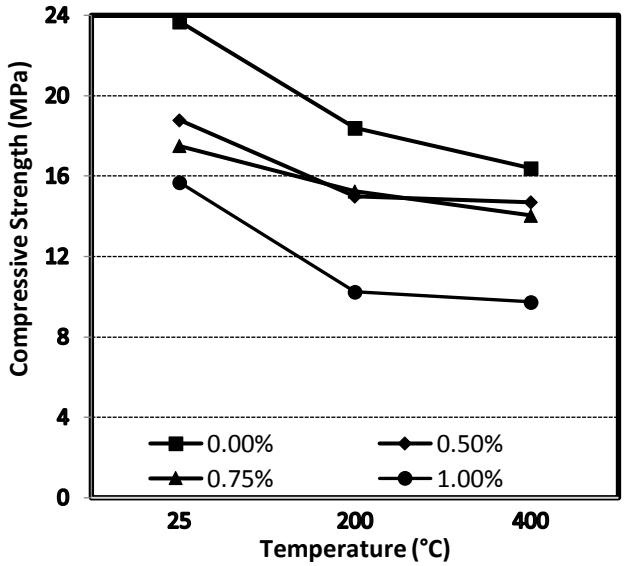

Fig. 19. Compressive strength at elevated temperature due to fibers.

Acknowledgements

None declared.

Funding

The authors received no financial support for the research, authorship, and/or publication of this manuscript.

Conflict of Interest

The authors declared no potential conflicts of interest with respect to the research, authorship, and/or publication of this manuscript.

References

ASTM C39 (2016). Standard Test Method for Compressive Strength of Cylindrical Concrete Specimens. ASTM International, West Conshohocken, PA.

ASTM C78 (2016). Standard Test Method for Flexural Strength of Concrete (Using Simple Beam with Third-Point Loading). ASTM International, West Conshohocken, PA.

ASTM C109 (2016). Standard test method for compressive strength of hydraulic cement mortars (Using 50-mm Cube Specimens). ASTM International, West Conshohocken, PA.

ASTM C143M-03. (2019). Standard Test Method for Slump of Hydraulic-Cement Concrete. ASTM International, West Conshohocken, PA.

ASTM C618 (2019). Specification for Coal Fly Ash and Raw or Calcined Natural Pozzolan for Use in Concrete. Annual Book of ASTM Standards, ASTM International, West Conshohocken, PA.

ASTM C1116 and C1399 (2015). Standard specification of fiber reinforced concrete and shortcrete, and test method for obtaining average residual strength for fiber reinforced concrete. ASTM International, West Conshohocken, PA.

Atoyebi OD, Odeyemi SO, Bello SA, Ogbeifun CO (2018). Splitting tensile strength assessment of lightweight foamed concrete reinforced with waste tyre steel fibers. *International Journal of Civil Engineering and Technology*, 9(9), 1129-1137.

Dawood ET, Alattar AA, Abbas WA, Mohammad YZ (2019). Behavior of foamed concrete reinforced with hybrid fibers and exposed to elevated temperatures. *Springer Nature Journal*, 2(1), 84.

E. S. S. 47651-1 (2013). Portland Cement, Ordinary and Rapid Hardening. Egyptian Organization for Standardization & Quality, Cairo, Egypt.

E. S. S. 1109 (2008). Aggregates for Concrete. Egyptian Organization for Standardization & Quality. Cairo Egypt.

E.P.C 203 (2018). Egyptian Practice Code for Design and Construction of Reinforced Concrete Structures, Ministry of Housing, Utilities & Urban Development, Egypt.

Falliano D, De Domenico D, Ricciardi G, Gugliandolo E (2019). Compressive and flexural strength of fiber-reinforced foamed concrete: Effect of fiber content, curing conditions and dry density. *Construction and Building Materials*, 198, 479-493.

Fu Y, Wang X, Wang L, Li Y (2020). Foam concrete: A state-of-the-art and state-of-the-practice review. *Advances in Materials Science and Engineering*, 1-25

Gencel O, Bilir T, Bademler Z, Ozbakkaloglu T (2022). A detailed review on foam concrete composites: Ingredients, properties, and microstructure. *Applied Sciences*, 12(11), 5752.

Gopalakrishnan R, Sounthararajan VM, Mohan A, Tholkapiyan M (2020). The strength and durability of fly ash and quarry dust light weight foam concrete. *Materials Today*: Proceedings, 22, 1117-1124.

Habsya C, Diharjo K, Setyono P, Satwiko P (2018). Physical, mechanical and thermal properties of lightweight foamed concrete with fly ash. *IOP Conference Series: Materials Science and Engineering*. 420(1), 012062.

Hazlin AR, Iman A, Mohamad N, Goh WI, Sia LM, Samad AAA, Ali N (2017). Microstructure and tensile strength of foamed concrete with added polypropylene fibers. *MATEC Web of Conferences*, 103, 01013.

Kanagalakshmi DA, Sasikumar K, Pravin EB (2015). An Investigation on foam concrete with quarry dust replacement for filler in mix design. *International Journal of Emerging Technology in Computer Science & Electronics*, 13(1), 570-581.

Karahan O, Durak U, İlkentapar S, Atabey İİ, Atiş CD (2019). Resistance of polypropylene fibered mortar to elevated temperature under different cooling regimes. *Revista de la Construcción*, 18(2), 386-397.

Kaya M, Köksal F (2021). Influences of high temperature on mechanical properties of fly ash based geopolymer mortars reinforced with PVA fiber. *Revista de la Construcción*, 20(2), 393-406.

Kearsley EP, Wainwright PJ (2001). Porosity and permeability of foamed concrete. *Cement and Concrete Research*, 31(5), 805-812.

Krishna AS, Siempu R, Kumar GS (2021). Study on the fresh and hardened properties of foam concrete incorporating fly ash. *Materials Today*: *Proceedings*, 46, 8639-8644.

Mydin MAO, Abdullah MMAB, Razak RA, Nawi MNM, Risdanareni P, Puspitasari P, Vizureanu P (2023). Study on Polypropylene twisted bundle fiber reinforced lightweight foamed concrete. *Buildings*, 13(2), 541.

Nambiar EK, Ramamurthy K (2006). Influence of filler type on the properties of foam concrete. *Cement and Concrete Composites*, 28(5), 475-480.

Othman R, Jaya RP, Muthusamy K, Sulaiman M, Duraisamy Y, Abdullah MMAB, Sandu AV (2021). Relation between density and compressive strength of foamed concrete, *Materials,* 14(11), 2967.

Raupit F, Saggaff A, Tan CS, Lee YL, Tahir MM (2017). Splitting tensile strength of lightweight foamed concrete with polypropylene fiber. *International Journal on Advanced Science, Engineering and Information Technology*, 7(2), 424.

Reddy AB, Punith A, Dongarkar K (2017). Effect of fly ash on strength properties of foam concrete. *International Journal of Latest Engineering Research and Applications*, 2(7), 7-12.

Roslan AF, Awang H, Mydin MAO (2013). Effects of various additives on drying shrinkage, compressive and flexural strength of lightweight foamed concrete (LFC). *Advanced Materials Research*, 626, 594-604.

Serudin AM, Mydin MAO, Ghani ANA (2019). Enhancement of mechanical properties of lightweight foamed concrete using fibermesh. *International Journal of Recent Technology and Engineering*, 8(2), 234-242.

Shi J, Liu Y, Liu B, Han D (2019). Temperature effect on the thermal conductivity of expanded polystyrene foamed concrete: Experimental investigation and model correction. *Advances in Materials Science and Engineering*, 2019(4), 1-9.

Soleimanzadeh S, Mydin MAO (2013). Influence of high temperatures on flexural strength of foamed concrete containing fly ash and polypropylene fiber. *International Journal of Engineering*, 26(2), 117-126.

Challenge Journal of Concrete Research Letters

Research Article

Performance of light weight ferrocement composite walls

Yousry B. I. Shaheen [a], Zeinab A. Etman [a], Doha E. A. Kandil [a,*]

[a] *Department of Civil Engineering, Menoufia University, Shebin ElKoum, Menofia, Egypt*

ABSTRACT

The aim of this research is to examine the performance of reinforced lightweight ferrocement walls under vertical and horizontal loading. The walls were made up of two thin layers of ferrocement reinforced with one, two, three, or four layers of welded wire mesh or expanded steel mesh. The panels' core was constructed of lightweight extruded foam. An experimental program of thirteen lightweight walls with total dimensions of 100x650x1250 mm was casted to achieve this goal and tested until failure. ABAQUS finite-element package was conducted. The parameters in this study were the kind of reinforcement; welded and expanded wire meshes, the steel bars, and. the number of layers of steel mesh. Ultimate load, mode of failure, initial cracking load, service load, energy absorption, and ductility ratio were calculated and observation to evaluate the findings. The findings displayed that the performance of the ferrocement walls reinforced with expanded wire meshes is better than that of the walls reinforced with welded wire meshes. The energy absorbed increased by 40 % for specimens reinforced with expanded wire meshes is more than that of the walls reinforced with welded wire a good agreement was observed among the theoretical and experimental observations. This paper highlights uses of employing light weight ferrocement units in building of economic housing, which is particularly valuable for both developed and developing nations, with significant frugal benefits.

ARTICLE INFO

Article history:
Received 29 April 2023
Revised 7 June 2023
Accepted 5 July 2023

Keywords:
Ferrocement
Welded mesh
Expanded mesh
Composite walls
Finite element method
ABAQUS

1. Introduction

Ferrocement is a composite material made up of a mortar matrix and a number of layers of steel mesh reinforcement embedded in the matrix. Shaheen et al. (2017) described a novel precast U-shape ferrocement form reinforced with metallic and non-metallic mesh reinforcement. The experimental program compares casting and testing ten slabs with total dimensions of 500x100x2500 mm that include 40 mm thick U shape permanent ferrocement forms. The testing program revealed that the suggested slabs could achieve high ultimate and serviceability loads, superior fracture resistance management, high ductility, and strong energy absorption qualities at a reasonable cost when compared to the control specimen.

Shaheen et al. (2021) assessed the experimental and theoretical calculation of ferrocement walls. Under concentric compressive stresses, twelve RC walls with dimensions of 450 mm x 100 mm x 1000 mm were tested. The factors under consideration include material k of reinforcing, the number of mesh layers, and the volume fraction of the reinforcement. The study's goal is to evaluate the effect of employing new revolutionary materials in reinforcing RC composite walls. Nonlinear analysis was used to emulate the behavior of tested specimens using the ANSYS-10.0 software. The parametric research is also explained in detail in order to investigate alterations that can be expect with different results with more variable, such as modifying the wall dimensions. The numerical findings obtained revealed that the FE simulation had an adequate accuracy in approximating the experimental values. Furthermore, the strength acquired by samples reinforced with welded steel mesh was 40% greater than that gained by those reinforced with expanded steel mesh. In comparison to ordinary reinforced concrete specimens, ferrocement specimens evaluated under axial compressive stresses demonstrate better ultimate loads and energy absorption capacity.

* *Corresponding author*. Tel.: +2-01-021-372820 ; E-mail address: engdohakandil@gmail.com (D. E. A. Kandil)
ISSN: 2548-0928 / DOI: https://doi.org/10.20528/cjcrl.2023.03.002

Shaheen et al. (2018) examined the performance of precast lightweight ferrocement walls and ANSYS14.5 was used as finite element package. The precast lightweight ferrocement hollow blocks of 200*400*200mm and filled with the core material the core material was hollow blocks. These blocks were arranged to form four walls that measured 840*650*250mm. The core material was investigated as one layer of welded steel mesh. Welded steel mesh was used as a bonding layer form to support the plastering in single, double, and three layers. The results show that the experimental results confirmed that better cracks resistance, high serviceability and ultimate loads, and good energy absorption could be improved using the proposed walls which verify the validity of used the proposed model.

Shaheen et al. (2019) examined the structural behavior of thin ferrocement plates exposed to axial compression loads with and without a frame. The theoretical model ANSYS15 was used. Twelve samples of 50 mm thick, 1000 mm wide, and 1000 mm long thin ferrocement plates were tested under compression stress till failure.

With particular attention devoted to first cracking, maximum load, deflection at different stages of loading, fracture pattern, energy absorption, and ductility index, the behavior of the tested thin plates was assessed. As well as increased deformation qualities, high strength, ductility, and energy absorption, a test specimen reinforced with three layers of welded steel wire steel meshes combined with seven steel bars as steel reinforcement (FS7W3) also showed these properties. A good agreement between the theoretical and experimental finds.

Shaheen et al. (2021) inspected the structural performance integrity of lightweight semicircular ferrocement composite roof panels. The suggested panels weight less than conventional reinforced concrete panels. Two thin layers of ferrocement reinforced with one or two layers of welded wire mesh closely together made up the sandwich panels. The core was constructed from low weight fibrous foam concrete. Shear was transferred among the two layer of ferrocement skin layers via the core in-between using steel wires from the two skin layers that were employed to connect the steel meshes and serve as shear connectors.

The skin of the ferrocement will be 25 mm thick. The core material, which will be 70 mm thick and made of pyrite and ad pour 55 as lightweight aggregate, will be 70 mm thick. To strengthen the skin, two types of steel mesh were employed. Welded wire mesh and expanded metal mesh are two examples. Steel wire shear connectors will be utilized to link the top and bottom skin layers, and also provide shear reinforcement. The panels were subjected to experimental testing. A total of 16 sandwich semicircular panels with dimensions of 500 mm in width and 2000 mm in length were tested up to failure under four lines loadings of span 1900 mm. the behavior of each panel in deformation and cracking were recorded and monitored. The final observation will be compared to theoretical ones using the ABAQUS finite elements software version 14. The findings will indicate that the suggested panels can achieve high ultimate and serviceability loads, fracture resistance management, a high ductility ratio, and superior energy absorption qualities.

Shaheen et al. (2022) studied the properties of lightweight ferrocement walls. The results show that the walls with expanded mesh had more ultimate load compared with walls reinforced with welded mesh.

Shaheen et al. (2023) examined the flexural behavior of ferrocement beam. They used fourteen beams with dimensions (1000, 100 and 150 mm) reinforced with welded and expanded meshes. All beams tested till failure under flexural load. They observed that ferrocement beams achieved high ultimate and serviceability loads, crack resistance, high ductility.

In this research we searched the performance of ferrocement walls under two loads (compressive and lateral) with core material as foam. On the other hand, the previous studies discussed the effect of one direction loading and some other core material like hollow block.

2. Research Significance

This work depicts light weight ferrocement walls that have been exposed to uniform axial compression and lateral loadings. As an alternative to traditional reinforcement, welded steel wire and extended steel wire networks are utilized. The essential goals of the experimental program detailed in this think about were to:

- Examine the performance of light weight ferrocement composite walls under uniform axial compression and lateral loadings.
- Investigating the influence of reinforcing kind and number of layers of steel wire meshes (one, two, three, and four layers.) on performance of ferrocement walls. ABAQUS, finite element tool, will undertake theoretical analysis to validate the experimental program's results.

3. Material Properties

Throughout the current study:

Aggregate sand was employed as the fine aggregate. Table 1 displays the results of a sieve analysis performed on the sand used in the ferrocement mortar mix.

CEMI 42.5 N was utilized, and its mechanical and physical qualities were examined for concrete works in accordance with E.S.S, 4756-11 (2013).

The water utilized for mixing and curing the examined specimens was pure drinking fresh water devoid of contaminants.

Polypropylene 300–e3 fibers were utilized. It was offered in Egyptian stores. It was employed in concrete mixtures to improve the properties of the concrete. Based on manufacturer guidelines, the proportion of increment was set at 900 gm/m^3. Table2 shows the properties of Polypropylene fibers 300-e3

A high range water reducer HRWR was employed as a super plasticizer. It was employed to increase the mix's workability. Sika Egypt provided it for Construction Chemicals in the concrete mix of walls. It satisfies the su-

per plasticizer criteria of ASTM-C-494 Types G and F and BS EN 934 Part 2: 2001.

Silica fume powder with a grey tint was utilized to replace some of the cement. Silica fume was employed to exchange 10% of the cement composition by weight. Table 3 displays the properties of silica fume.

Steel reinforcement as reinforcing bar, mild steel 8 mm in diameter was employed.

Expanded metal mesh was used to strengthen ferrocement channels. The weight of expanded wire mesh per m^2 was 1500 gm.

The galvanized welded metal mesh utilized in this project was acquired from China. As reinforcement for ferrocement channels, welded metal mesh was employed. The m^2 of welded weir mesh was recorded 450 gm in weight.

Foam is a blue board (1.25x0.6x0.5 m) created using a continuous extrusion technique, with unique qualities such as low thermal conductivity, strong resistance to water penetration, high compressive strength, and a density of 36.5 kg/m^3.

Table 1. Results of the sieve analysis for fine aggregates.

Sieve diameter (mm)	4.75	2.83	1.41	0.707	0.354	0.177
Pass (%)	97.7	89.7	67.5	49	3.8	1.6

Table 2. Properties of Fiber mesh 300–e3.

Absorption	Nil
Specific gravity	0.91 gm/cm3
Fiber length	Single cut lengths
Electrical conductivity	Low
Acid and salt resistance	High
Melt point	324°F (162°C)
Thermal conductivity	Low
Ignition point	1100°F (593°C)
Alkali resistance	Alkali proof

Table 3. Chemical composition of silica fume.

Chemical	SiO_2	C	Fe_2O_2	CaO	Al_2O_2	MgO	MnO	K_2O	Na_2O
Weight (%)	92-94	3-5	0.1-0.5	0.1-0.15	0.2-0.3	0.1-0.2	0.008	0.1	0.1

4. Experimental Program

The experiment was carried out on thirteen walls. All test specimens had the same concrete proportions, with a total height of 1250 mm and cross sectional dimensions of 100x650 mm. Table 4 includes information on the test specimens. The specimens was designed by code, CO for the control wall which reinforced with steel bars, while the code W respect the wall reinforced with welded mesh, as well as the code WS for walls reinforced with welded mesh with steel bar, E the code of walls which reinforced by expanded mesh, moreover the code ES were reinforced by expanded mesh with steel bar. In addition, the number refers to the count of the layer.

4.1. Reinforcement details

The following figures showing the reinforcement details of all specimens in Figs. 1-5.

4.1.1. Reinforcement details of control wall (CO)

This group consist of the control wall. This wall was reinforced with four mild steel bars of 8 mm diameter in each side 4Ø8mm as shown in Fig. 1.

Table 4. Details of the test specimens.

Name	Type	Description
CO	Control	4 Φ 8 m
W2	Welded mesh	2 layer u & b
W3		3layer u & b
W4		4layer u & b
WS2	Welded mesh with steel bars	2layer u & b &4 Φ 8
WS3		3layer u & b & 4 Φ 8
WS4		4layer u & b & 4 Φ 8
E1	Expanded mesh	1layer u & b
E2		2layer u & b
E3		3layer u & b
ES1	Expanded mesh with steel bars `	1layer u & b & 4 Φ 8
ES2		2layer u & b & 4 Φ 8
ES3		3layer u & b & 4 Φ 8

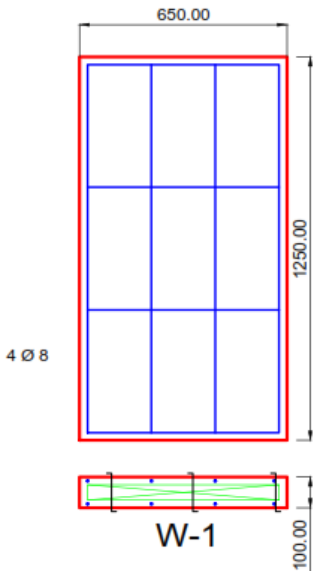

Fig. 1. Reinforcement details of control wall (CO).

4.1.2. Reinforcement details of Group-1 walls (W2, W3 and W4)

This group consist of three walls. The walls in this group are reinforced with welded steel mesh as well as W2 reinforced with two layer of welded steel mesh in each side, W3 reinforced with three layer of welded steel mesh in each side, and W4 reinforced with four layer of welded steel mesh in each side as shown in Fig. 2.

4.1.3. Reinforcement details of Group-2 walls (WS2, WS3 and WS4)

This group consist of three walls. The walls in this group were reinforced with welded steel mesh with steel bar as well as WS2 reinforced with two layer of welded steel mesh plus 4 Φ 8 in each side, WS3 reinforced with three layer of welded steel mesh plus 4 Φ 8 in each side and WS4 reinforced with four layer of welded steel mesh plus 4 Φ 8 in each side as shown in Fig. 3.

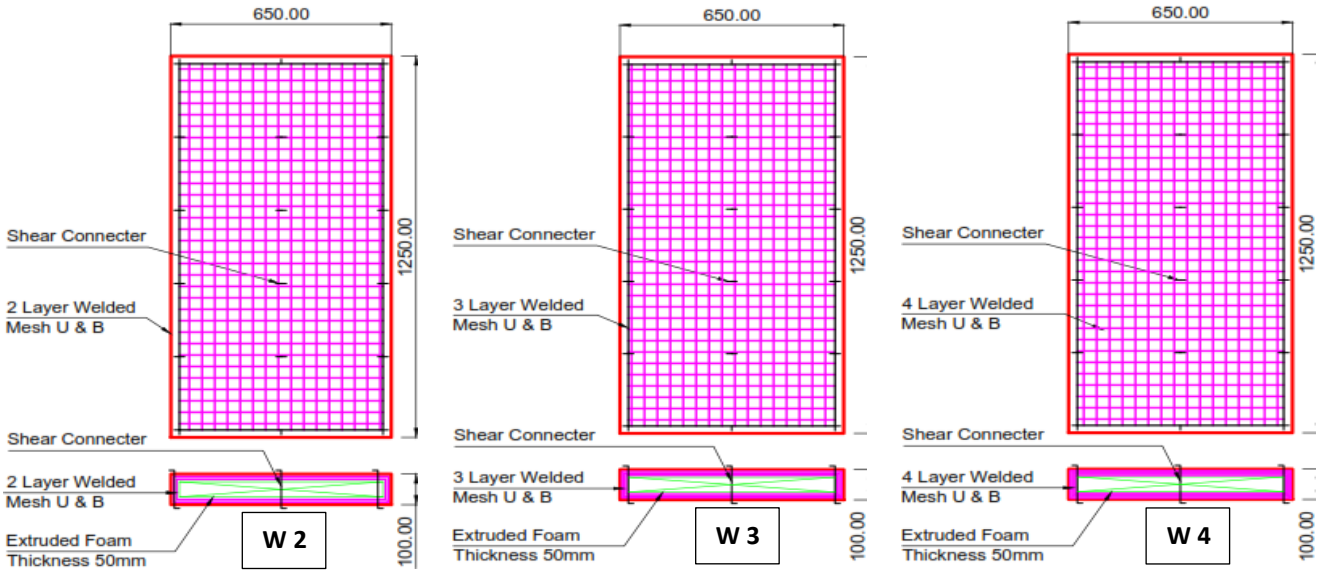

Fig. 2. Reinforcement details of Group-1 walls (W2, W3 and W4).

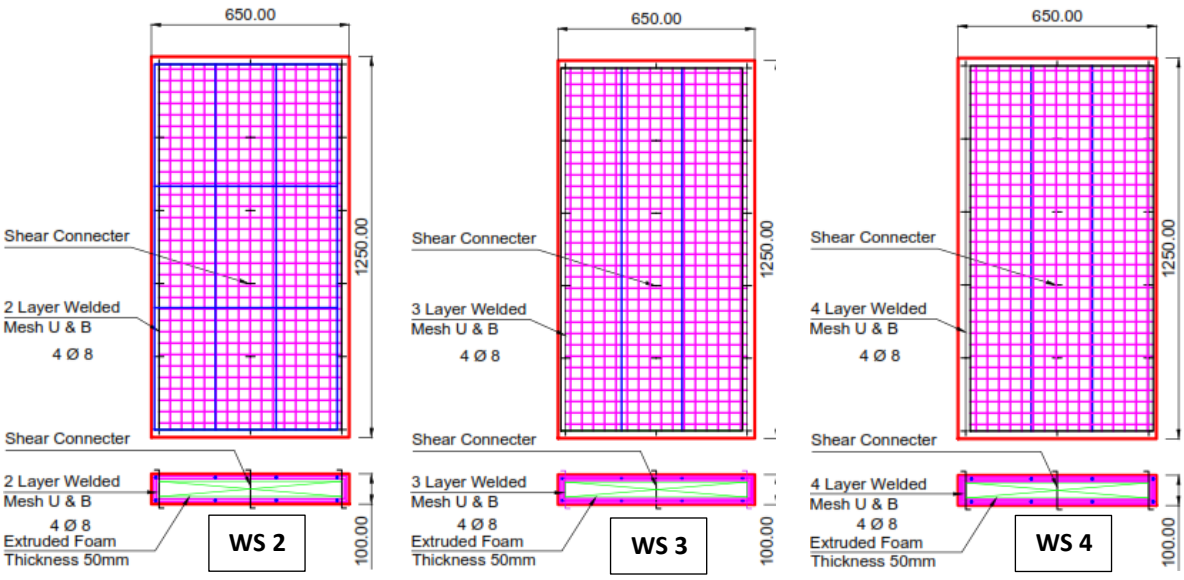

Fig. 3. Reinforcement details of Group-2 walls (W2, W3 and W4).

4.1.4. Reinforcement details of Group-3 walls (E1, E2 and E3)

This group consist of three walls. The walls in this group were reinforced with expanded steel mesh as well as E1 reinforced with one layer of expanded steel mesh in each side, E2 reinforced with two layers of expanded steel mesh in each side and E3 reinforced with three layers of expanded steel mesh in each side as shown in Fig. 4.

4.1.5. Reinforcement details of Group-4 walls (ES1, ES2 and ES3)

This group consist of three walls. The walls in this group are reinforced with expanded steel mesh with steel bars as well as ES1 reinforced with one layer of expanded steel mesh plus 4 Φ 8 in each side, ES2 reinforced with two layers of expanded steel mesh plus 4 Φ 8 in each side and ES3 reinforced with three layers of expanded steel mesh plus 4 Φ 8 in each side as shown in Fig. 5.

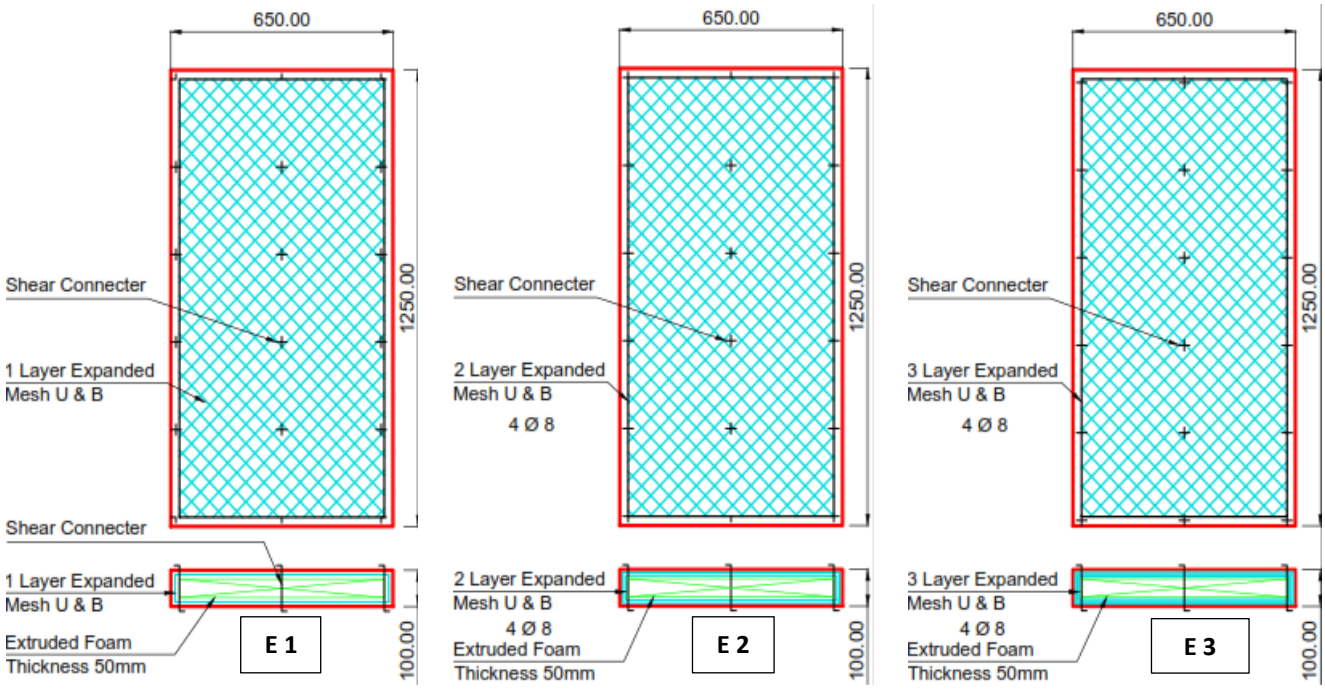

Fig. 4. Reinforcement details of Group-3 walls (E1, E2 and E3).

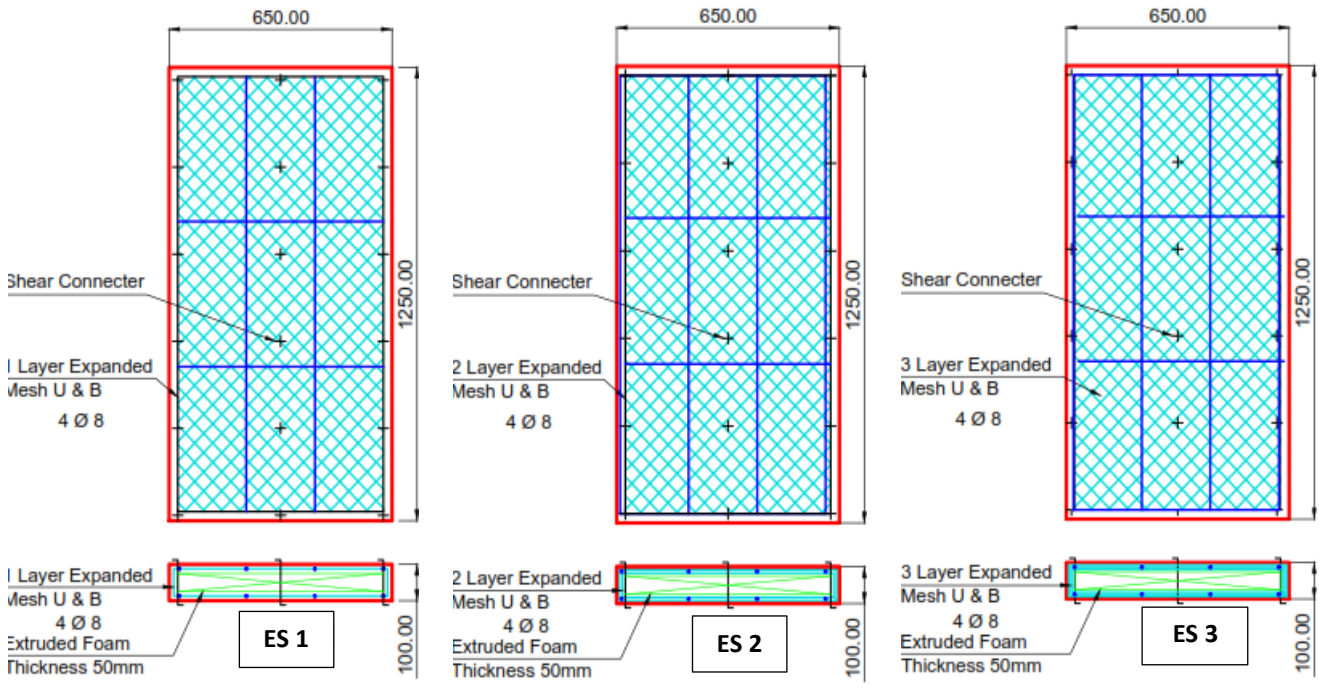

Fig. 5. Reinforcement details of Group-4 walls (ES1, ES2 and ES3).

4.2. Preparation of the reinforcement

There were some photo of preparation of reinforcement details of walls.

4.3. Design mix

The concrete mortar which was used of casting specimens was designed to have an ultimate compressive strength of 35 MPa after 28 days. The mortar matrix mix characteristics were determined using the ACI Committee 549 Report (1988). It was content of initially dry mixed before adding water and remixing the entire patch in the mixer. For all specimens, mechanical compaction was used. Table 5 shows the mix proportions by (kg\m^3). 15 cubes; 150 ×150 ×150 mm were cast and tested to determine the compressive strength of the mix at 7 and 28 days according to E.S.S. (2011).

Fig. 6. Preparation of the reinforcement.

Table 5. Mix design of the ferrocement mortar mix.

Component	Portland cement	Sand	Silica fume	Water	Super plasticizers	Polypropylene 300–e3
Amount (kg/m^3)	650	1300	65	227	6.5	0.9

The walls were installed by arranging the reinforcement. The reinforcements were then put in the molds. Then, the mortar was mixed by combining the sand and cement in dry form, then adding polypropylene fiber mesh after that, adding the slurry (silica fume, water and super plasticizer).

The whole mixing time was around 10 minutes, which was sufficient to produce a homogenous mixture. The mixture was then poured into the wooden shape. The walls were meticulously compressed to achieve complete compaction. After the molds were filled with concrete, the surface of the concrete in the molds was smoothed using a trowel. Finally, the walls were kept in the forms for 24 hours in laboratory settings before being scraped away.

4.4. Casting of concrete mix

Fig. 7 shows the photo for casting of concrete.

Fig. 7. Casting of concrete mix.

4.5. Test set-up

Four LVDT were mounted to follow the vertical and horizontal displacement, three displacement transducers (type P1) with gauge lengths of 200 mm, two were mounted in the middle of the front face and the third in the side face of the test specimen. All test specimens were tested to failure under concentric loadings at the wall ends. Loading Cells, and Testing Frame are the key components of the testing facility.

The force was added progressively with increments ranging from 5.0 to 20 kN for all test specimens, and once the vertical load reached 5 kN, the horizontal load was gradually applied, as indicated in Fig. 8(a,b). At all loading phases, all deformation properties, cracking patterns, and strengths were comprehensively measured. The walls were progressively loaded at two spots through a loading steel beam. As a result, the wall was loaded up to failure in stages. A load cell with a capacity of 3500 kN was used to measure the load on the wall. Following each loading phase, the vertical mid-span deflections (V1), vertical side deflections (V2), horizontal displacement (H1), Pi-gauge readings, and generated normal stresses were recoded and recorded using an automated data logger device (TDS-150). Tanta University's reinforced concrete and heavy structures lab.

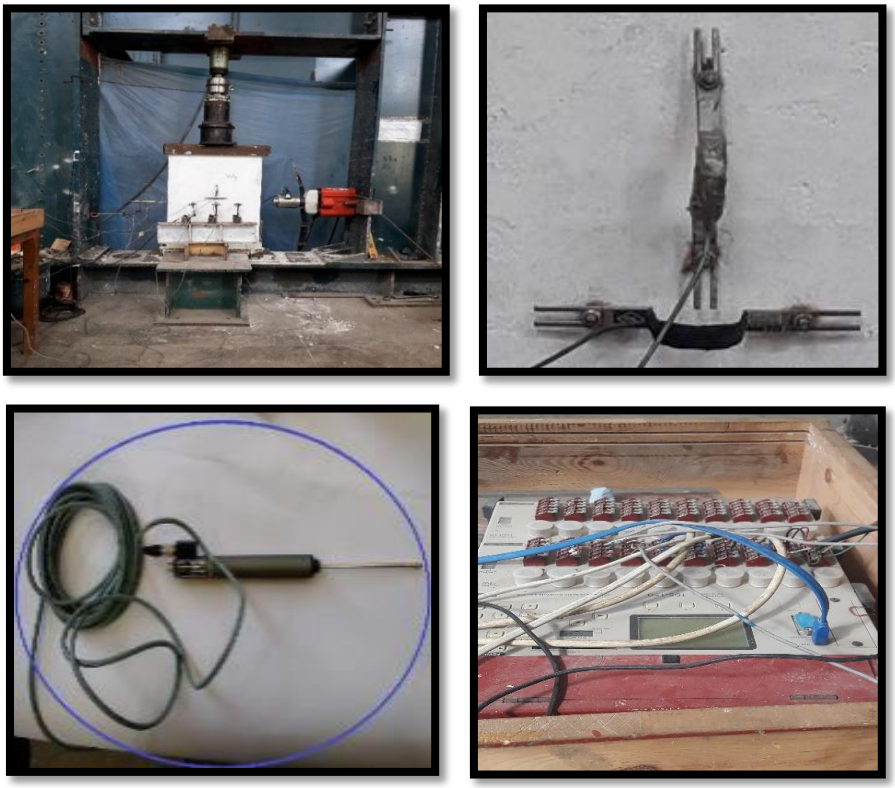

Fig. 8(a). Test set up and data logger unit used for the tests (TDS-150).

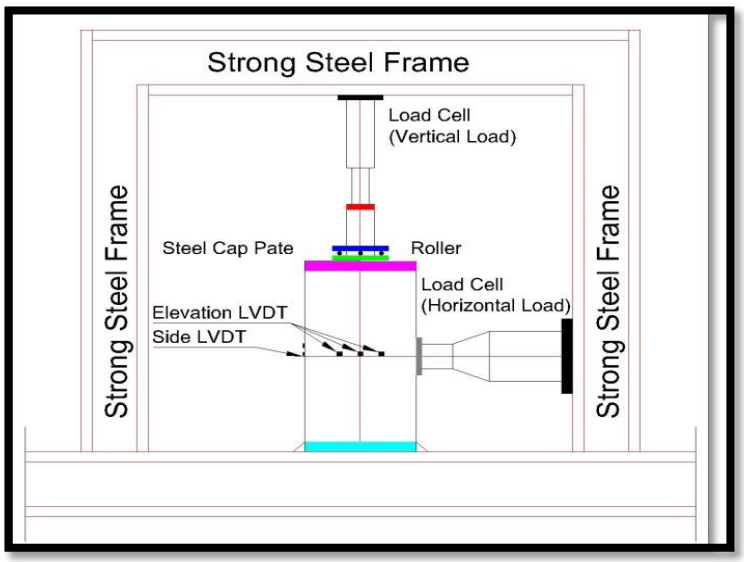

Fig. 8(b). Test set up in the vertical and horizontal loading test.

5. Experimental Results and Discussions

The findings for the initial loading, service load, vertical and horizontal displacement at ultimate load, ductility ratio, and energy absorption are shown in the Table 6. The first fracture load was calculated from the load deflection curve at the point when it began to depart from the linear relationship. The area under the load-deflection curve is sometimes used to define energy absorption. Figs. 9 and 10 show the first crack load and ultimate load.

5.1. Serviceability load

The serviceability load was computed using the CP110 equation: service load = (Experimental load - 1.4 D.L)/1.6 where the experimental load equals the greatest load achieved as shown in Fig. 11.

5.2. Ductility ratio

The ductility proportion was assessed by comparing the extreme stack mid-height uprooting to the starting breaking loads. When compared to divider CO, dividers fortified with extended metal work and welded steel work had a more prominent ductility proportion. Fig. 12 depicts the ductility proportions for all light weight dividers assessed.

5.3. Energy absorption

The energy absorption was calculated by computing the area under the load displacement curve for each wall, Energy = $\int_{u}^{\Delta u} f(\Delta) d\,\Delta$.

Walls strengthened with expanded steel mesh absorbed more energy than the control wall CO. Fig. 13 stresses energy absorption for all walls examined. Higher ductility and energy absorption are extremely beneficial in dynamic applications.

Table 6. Experimental results of vertical loading test for shear walls.

Wall	First crack V load (kN)	Ultimate V load (kN)	Serviceability V load (kN)	First crack H load	Ultimate H load (kN)	First crack V displacement (mm)	Maximum deflection (mm)	Ductility ratio	Energy absorption (kN.mm)
CO	112	185.30	115.72	68.34	98	0.541	2.20	4.06	283.55
W2	123	169.18	105.68	30	41	0.652	1.37	2.10	156.54
W3	133	182.24	113.83	50	74	1.07	1.93	1.80	244.30
W4	146	196.86	122.97	66	81	1.33	2.31	1.73	295.98
WS2	161	210.12	131.22	77	109	1.18	2.34	1.98	352.73
WS3	174	225.41	140.78	89	123	1.23	2.23	1.81	321.68
WS4	190	240.84	150.42	89	150	1.42	2.57	1.80	453.08
E1	143	190.77	119.15	72	95	1.24	2.17	1.91	315.86
E2	171	226.10	141.22	78	111	1.45	2.41	1.64	387.71
E3	180	230.18	143.77	80	115	1.72	2.64	1.30	413.87
ES1	181	250.24	156.30	50	105	1.54	2.57	1.72	427.96
ES2	209	287.30	179.44	52	144	2.02	3.35	1.62	703.63
ES3	241	290.35	181.33	64	155	2.42	4.43	1.48	922.47

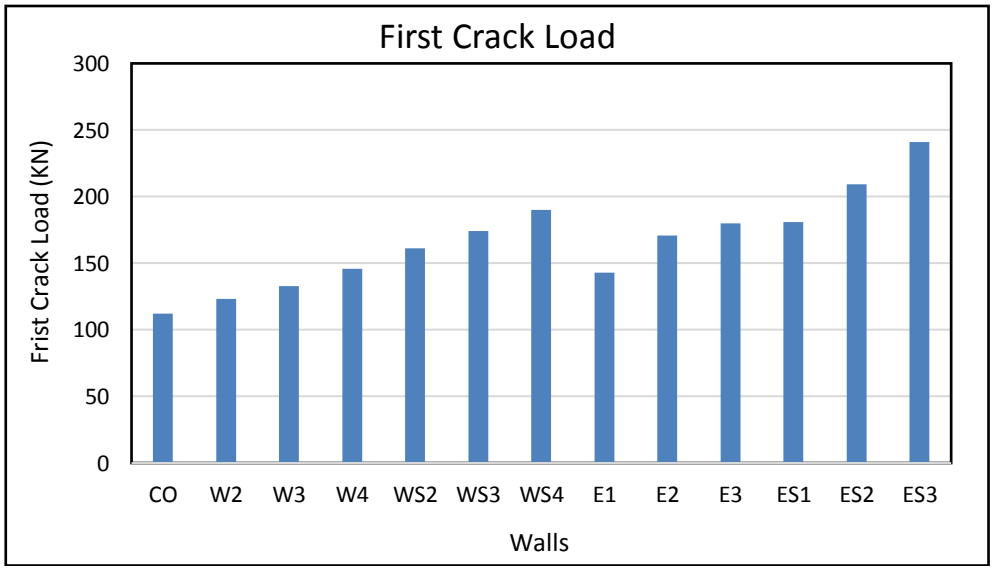

Fig. 9. First crack of tested of tested walls under vertical and horizontal loading.

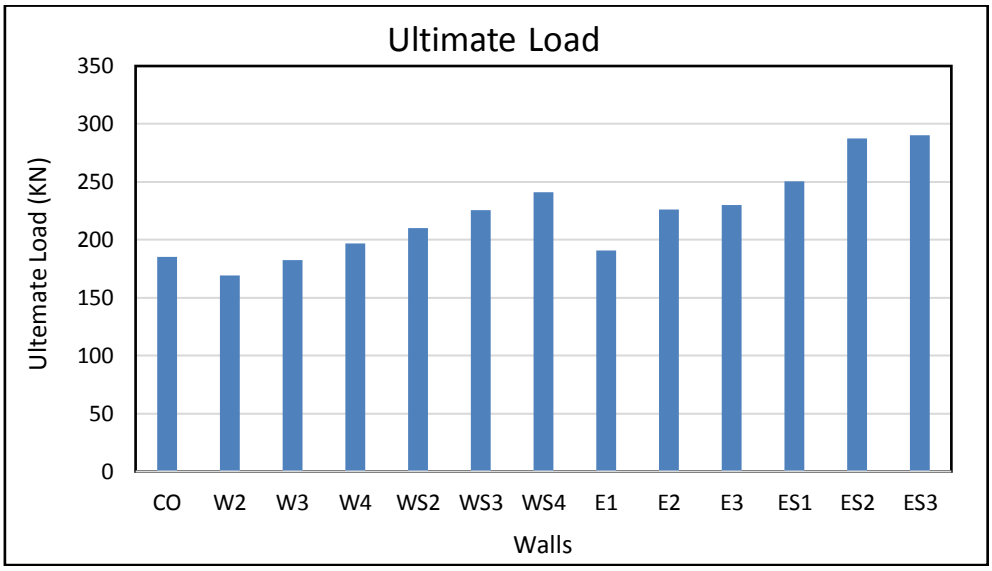

Fig. 10. Ultimate load of tested walls under vertical and horizontal loading.

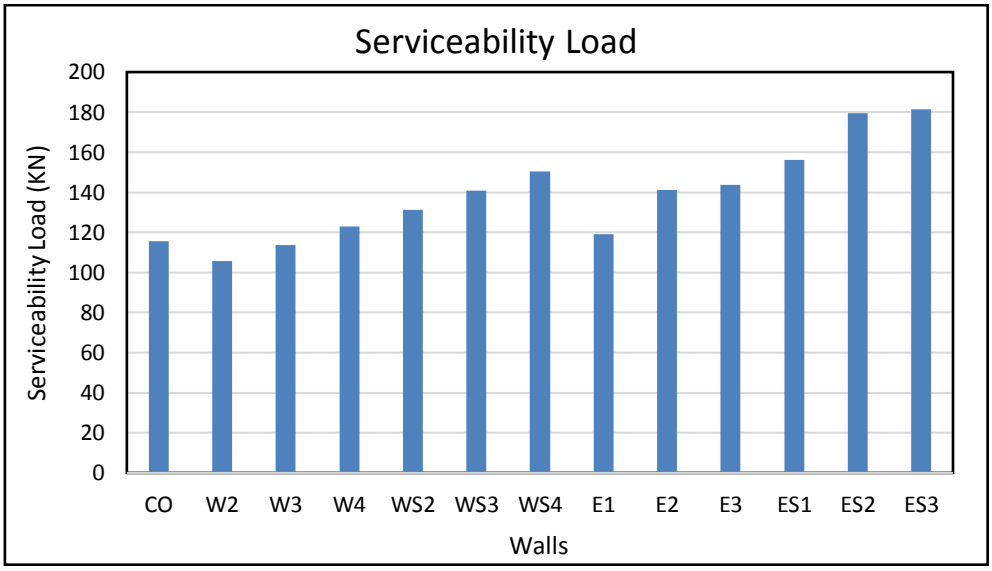

Fig. 11. Serviceability load of tested walls under vertical and horizontal loading.

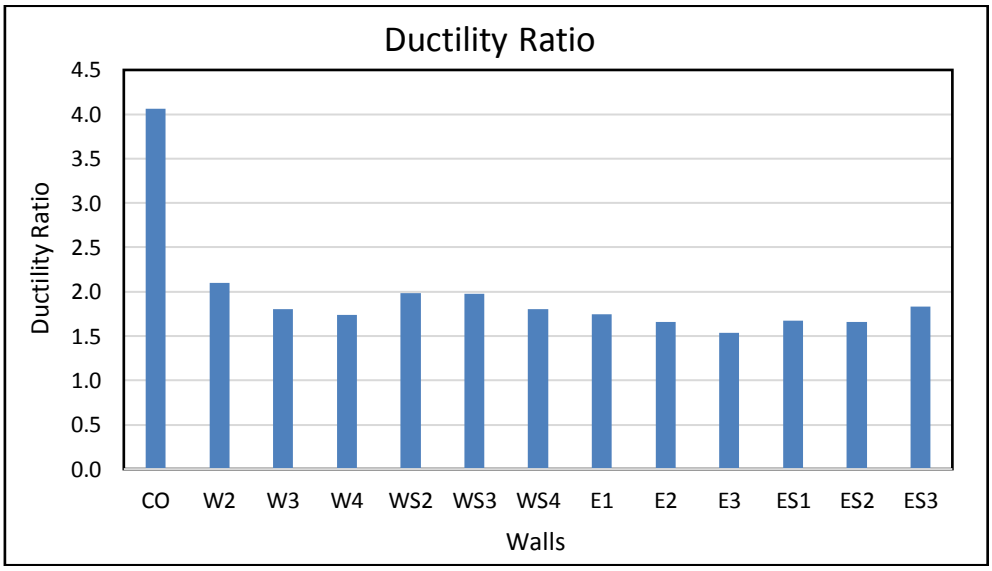

Fig. 12. Ductility ratio of tested walls under vertical and horizontal loading.

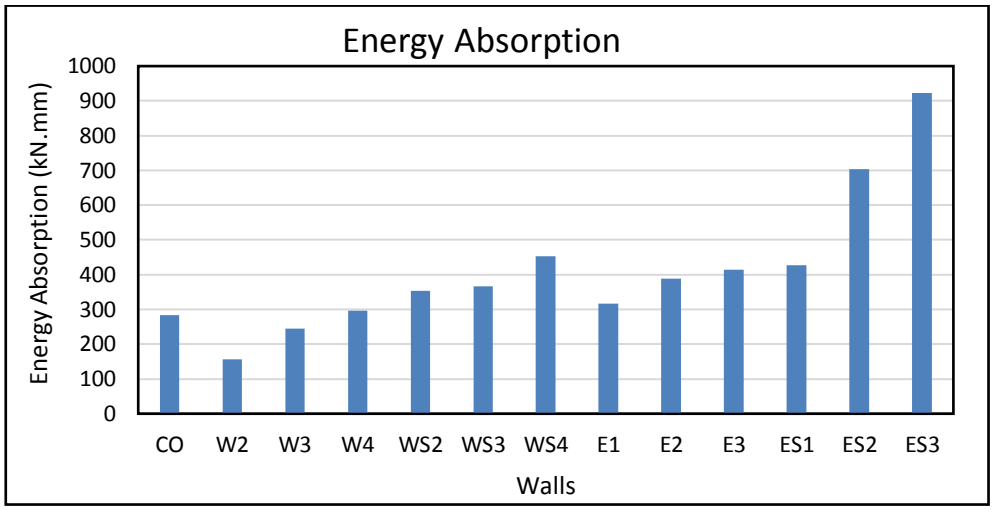

Fig. 13. Energy absorption of tested walls under vertical and horizontal loading.

5.4. Effect of type of reinforcement

Figs. 9, 10 and 13 depict the influence of several forms of reinforcement on the behavior of the tested walls. According to these results, the loads for control wall reinforcement with steel alone were the lowest when compared to walls reinforced with steel wire mesh alone or with steel wire mesh plus steel reinforcement. However, the energy absorption for walls reinforced with steel wire. meshes is higher than that for walls reinforced with steel reinforcement by 4%, 60%, 45%, &d 225% W4, WS4, E3, & ES3, respectively, when compared to CO.

Furthermore, as compared to CO, the ultimate load rose by 5%, 29%, 24%, & 56% for W4, WS4, E3 and ES3, respectively. When compared to CO, the first fracture load rose by 30%, 69%, 60%, & 115% for W4, WS4, E3 and ES3, respectively.

5.5. Effect of number of layer of reinforcement

Figs. 14-16 indicate the influence of the number of steel wire mesh layers. The initial cracking, maximum load, and energy absorptions increased as the quantity of welded steel wire mesh increased. In the case of welded steel mesh reinforced walls, the initial cracking load increased by 8% & 18% for three and four steel wire mesh layers (W3, W4) compared to two wire mesh layers, ultimate load increased by 7% and 12% for three and four steel wire mesh layers (W3, W4) compared to two wire mesh layers, and energy absorption increased by 62% and 96% for three and four steel wire mesh layers (W3, W4) compared to two wire mesh layers.

The initial cracking, ultimate load, and energy absorptions increased as the number of expanded steel wire mesh increased. In the case of walls reinforced with expanded steel mesh, the initial cracking load increased by 19% & 25% for two and three steel wire mesh layers (E2, E3) compared to one wire mesh layer, the ultimate load increased by 18% and 21% for two and three steel wire mesh layers (E2, E3) compared to one wire mesh layer, and energy absorption increased by 22% and 31% for two and three steel wire mesh layers (E2, E3) compared to one wire mesh layers.

5.6. Effect of presence of steel bars

Figs. 14-17 indicate the effect of the presence of steel bars with wire mesh. The first cracking, maximum load, and energy absorptions of the walls increased as the walls were strengthened with welded steel wire mesh and steel bars. The first cracking load rose by 30%, 28%, and 30% for walls reinforced with welded steel mesh and steel bars (WS2, WS3 and WS4), respectively, as compared to walls reinforced with welded steel mesh only (W2 ,W3 and W4),

Ultimate load increased by 24%, 23%, and 26% for walls reinforced with welded steel mesh with steel bars (WS2, WS3, and WS4) compared to walls reinforced with welded steel mesh only (W2,W3 and W4), and energy absorption increased by 134%, 131%, and 153% for walls reinforced with welded steel mesh with steel bars (WS2, WS3 and WS4).

The first cracking, maximum load, and energy absorptions of the walls increased as the walls were strengthened with expanded steel wire mesh and steel bars. When compared to walls reinforced with welded steel mesh only, the first cracking load rose by 26%, 22%, and 33% for walls reinforced with expanded steel mesh with steel bars (ES1, ES2 and ES3) (E1 ,E2 and E3), ultimate load increased by 31%,26%, and 26% for walls reinforced with expanded steel mesh with steel bars (ES1, ES2 and ES3) compared to walls reinforced with expanded steel mesh only (E1 ,E2 and E3), and energy absorption increased by 35%,81%, and 123% for walls reinforced with expanded steel mesh only.

5.7. Effect of using various types of meshes

Figs. 18-21 demonstrate the effect of employing different types of meshes. When a wall was reinforced with two layers of welded steel wire mesh against a wall reinforced with two layers of expanded steel wire mesh (W2, E2), the first cracking, maximum load, and energy absorptions increased. The initial cracking load rose by 39%, the maximum load by 24%, and energy absorption by 185%. When a wall was reinforced with three layers of welded steel wire mesh against a wall reinforced with

three layers of expanded steel wire mesh (W3, E3), the first cracking, maximum load, and energy absorptions increased. The initial cracking load rose by 35%, the maximum load by 26%, and energy absorption by 69%. Similarly, by reinforcing with various types of wire meshes and steel bars), the initial cracking, maximum load, and energy absorptions are increased as reported by Shaheen et al. (2023).

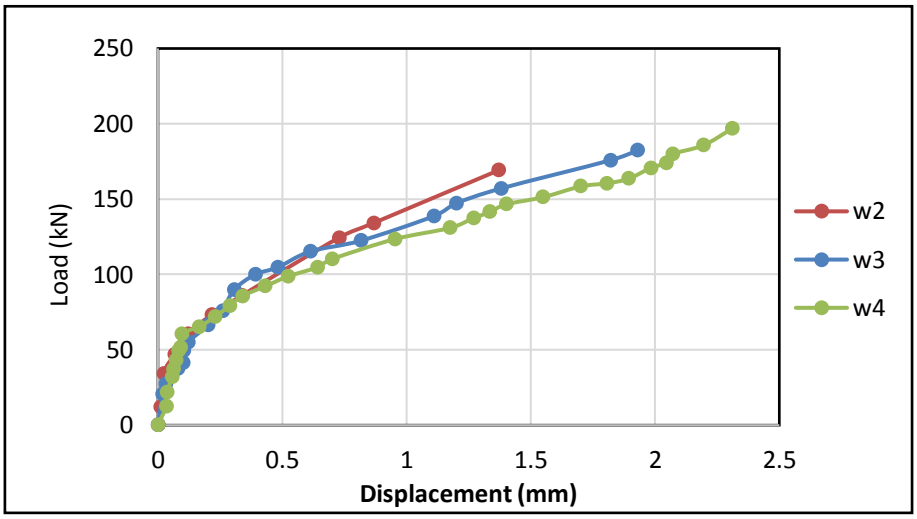

Fig. 14. Load-vertical displacement for Group-1.

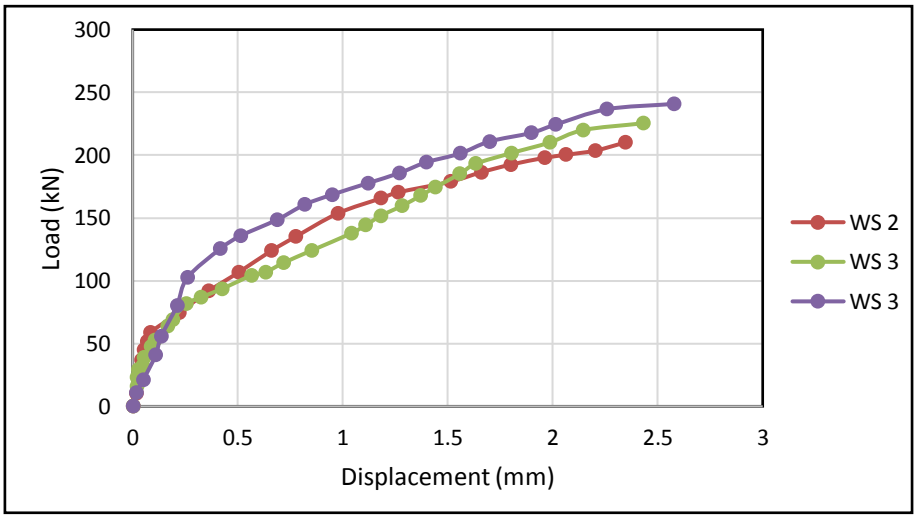

Fig. 15. Load-vertical displacement for Group-2.

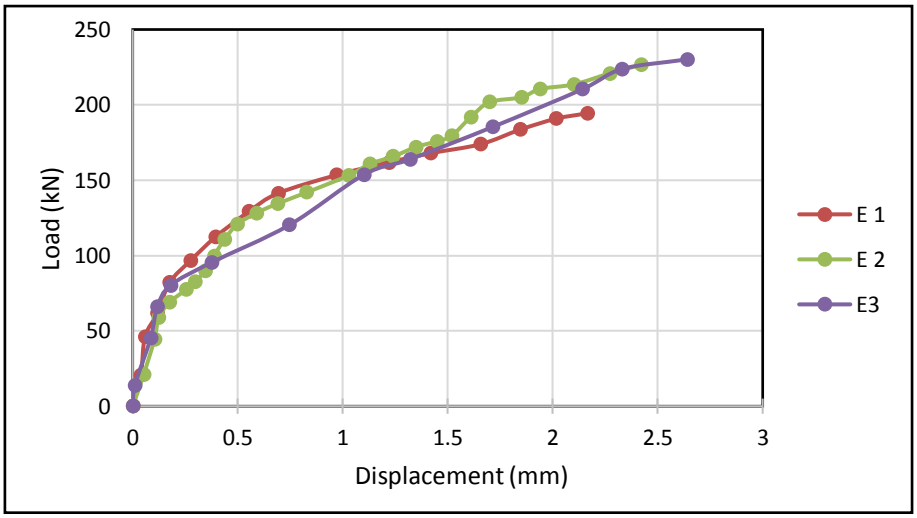

Fig. 16. Load-vertical displacement for Group-3.

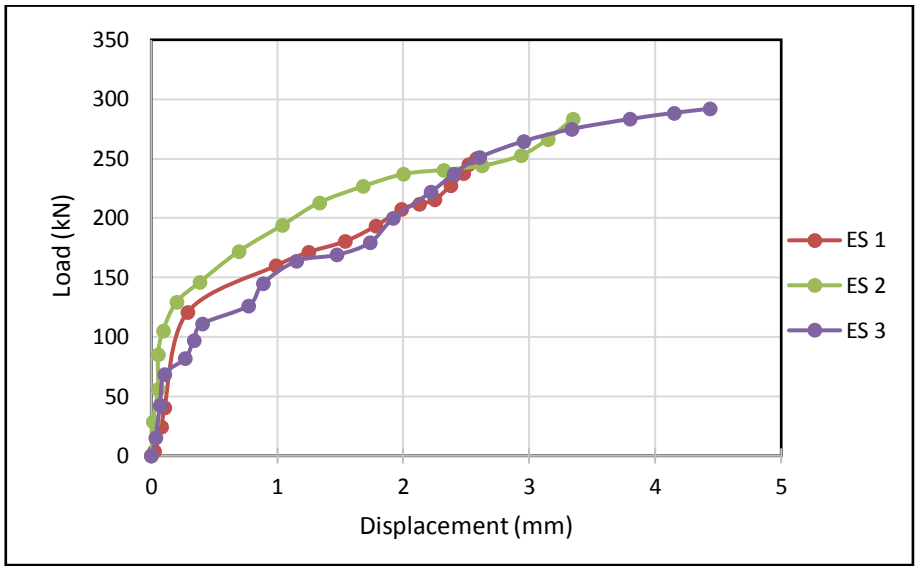

Fig. 17. Load-vertical displacement for Group-4.

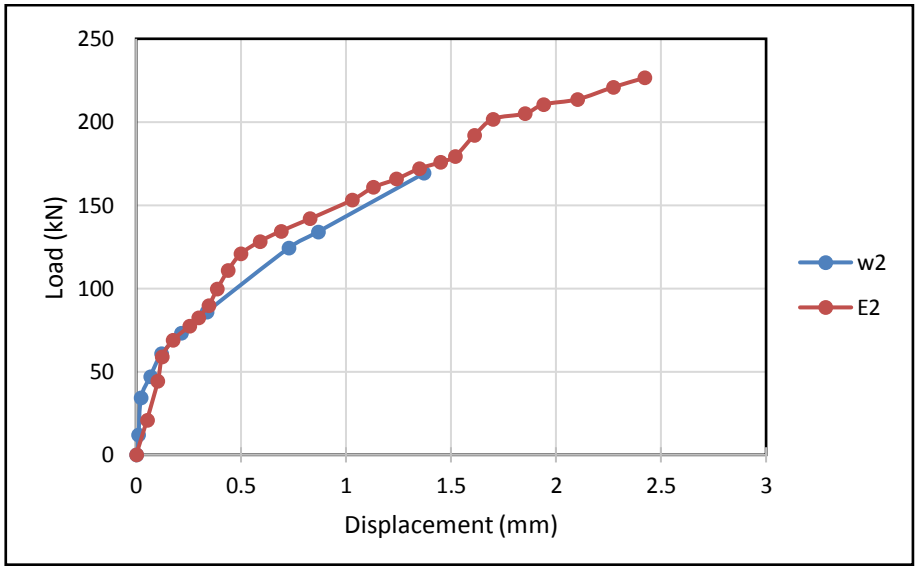

Fig. 18. Load-vertical displacement for W2 and E2.

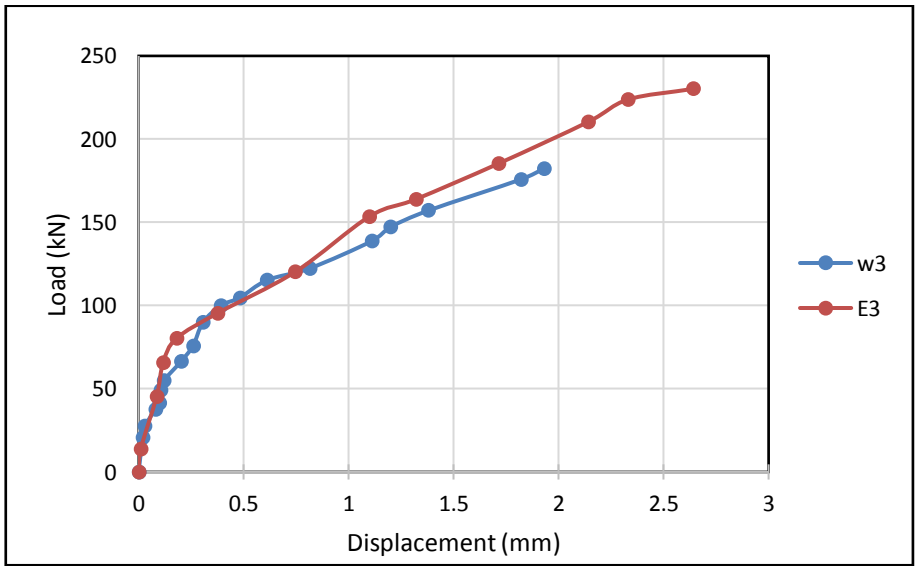

Fig. 19. Load-vertical displacement for W3 and E3.

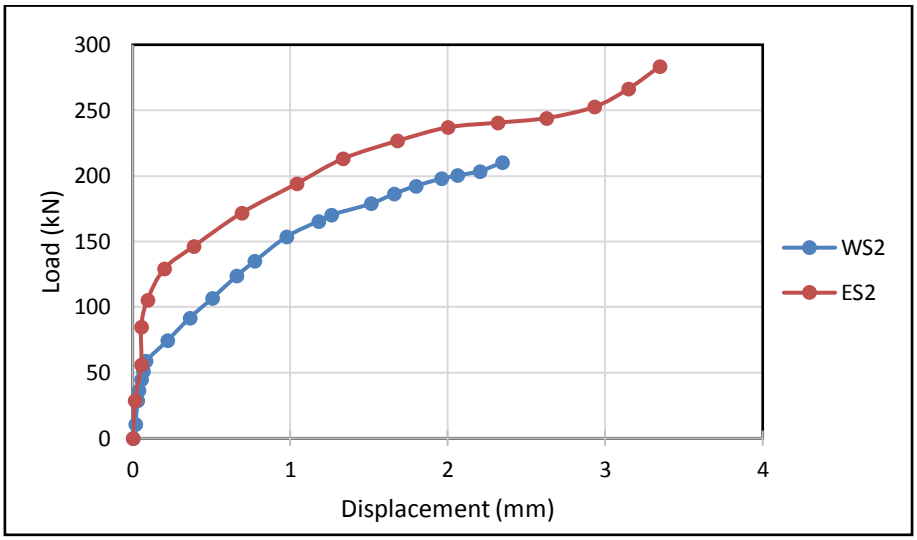

Fig. 20. Load-vertical displacement for WS2 and ES2.

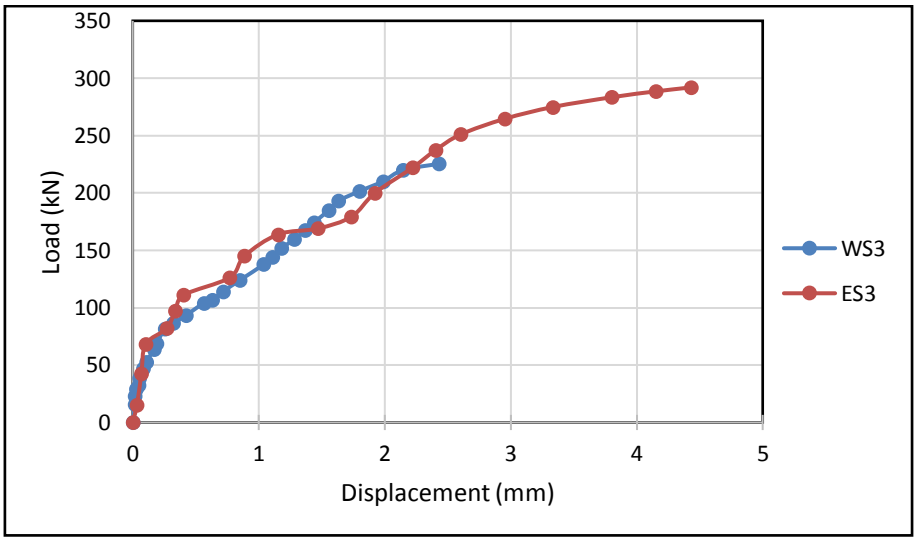

Fig. 21. Load-vertical displacement for WS3 and ES3.

5.8. Load-strain relationship

The load-strain curves for all tested walls were shown in Figs. 22-26 for all walls, the relationship among the load and strain was almost linear till the first crack load then it started to deviate from the linear relation.

5.9. Cracking behavior

Fig. 27 shows cracking patterns of all the tested light weight walls subject to compression and lateral loadings. We can observe the function of specific surface area of reinforcing and the presence of mesh reinforcement, to control crack width.

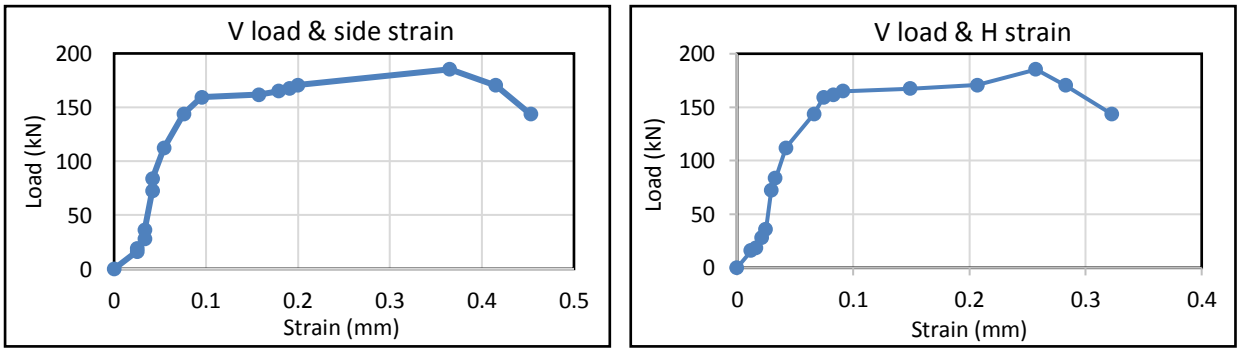

Fig. 22. Load-horizontal and -side strain for CO.

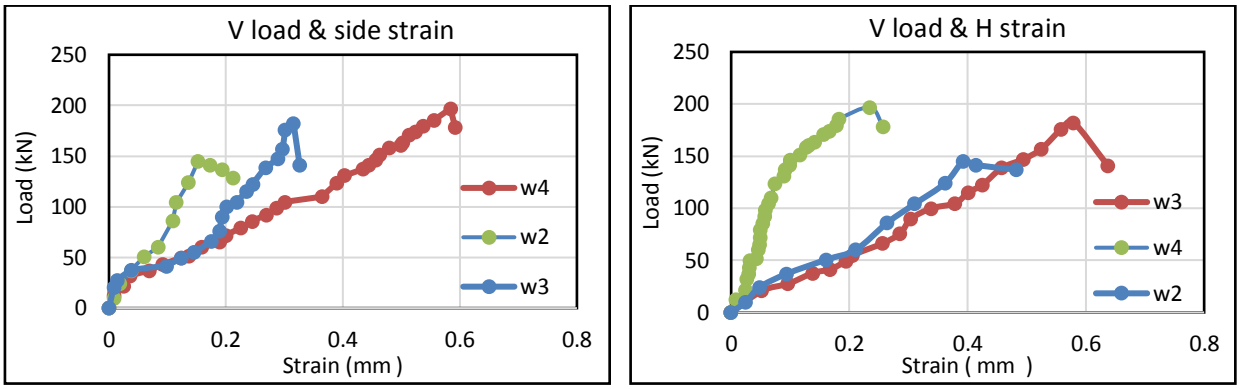

Fig. 23. Load-horizontal and -side strain for W2, W3 and W4.

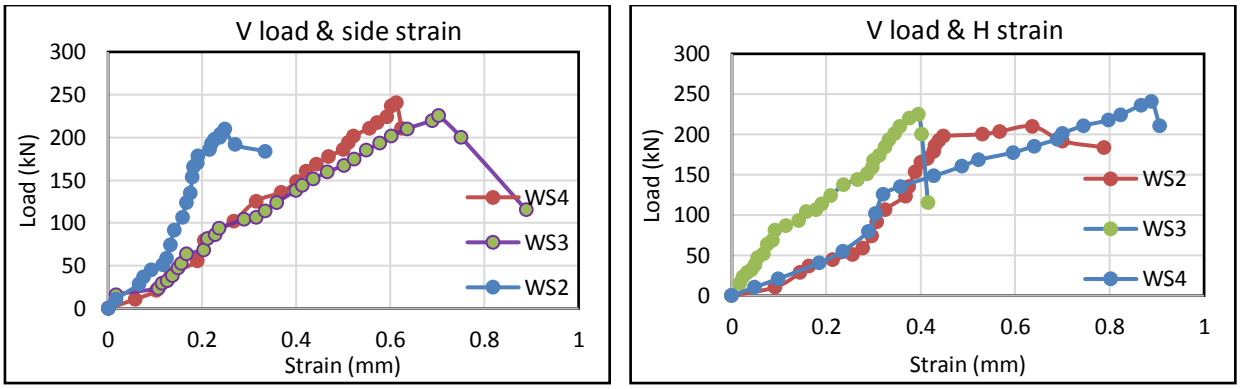

Fig. 24. Load-horizontal and -side strain for WS2, WS3 and WS4.

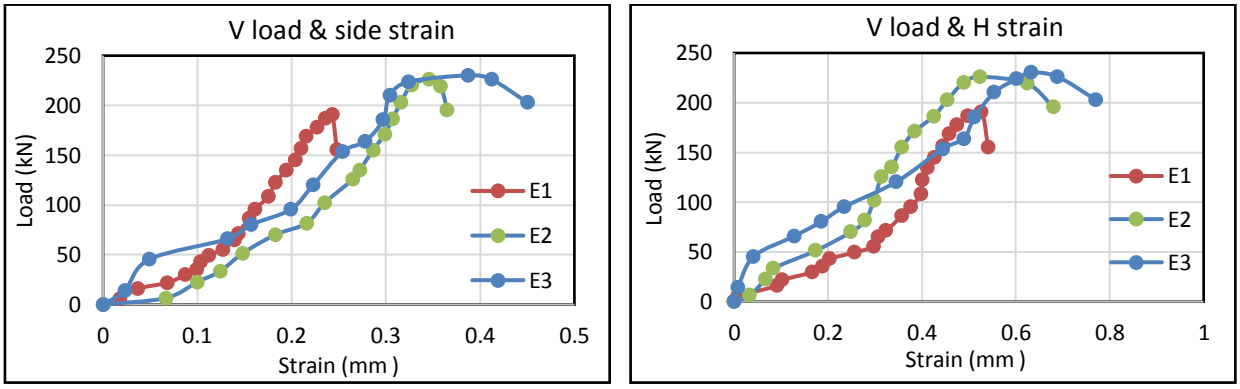

Fig. 25. Load-horizontal and -side strain for E1, E2 and E3.

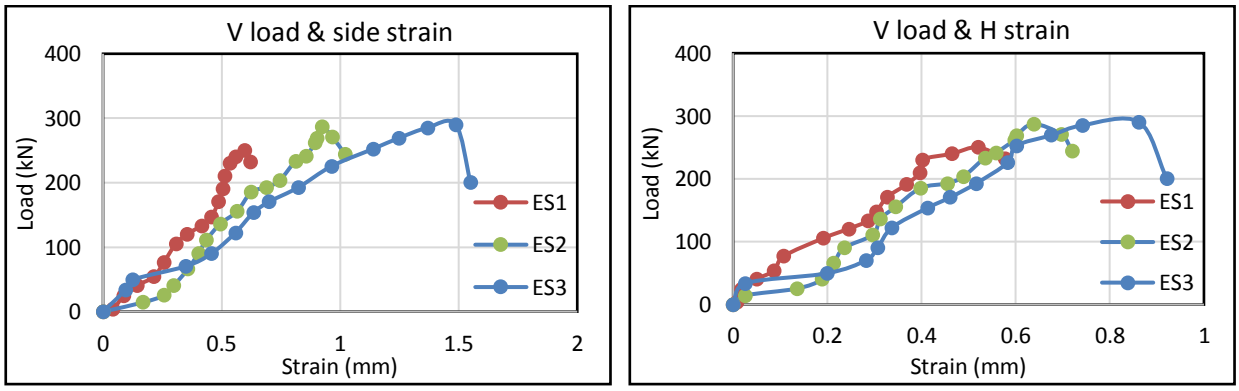

Fig. 26. Load-horizontal and -side strain for ES1, ES2 and ES3.

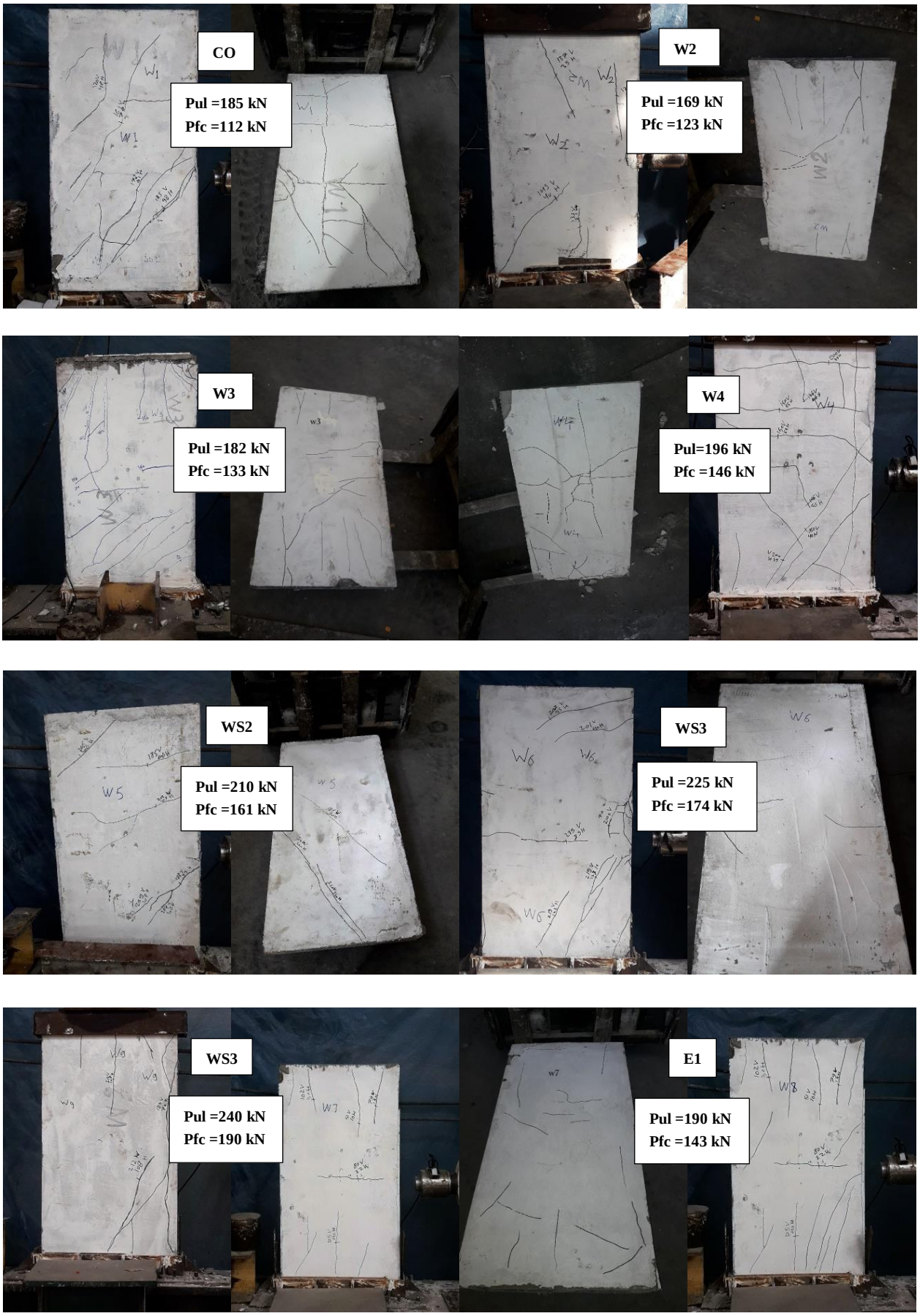

Fig. 27. (continued)

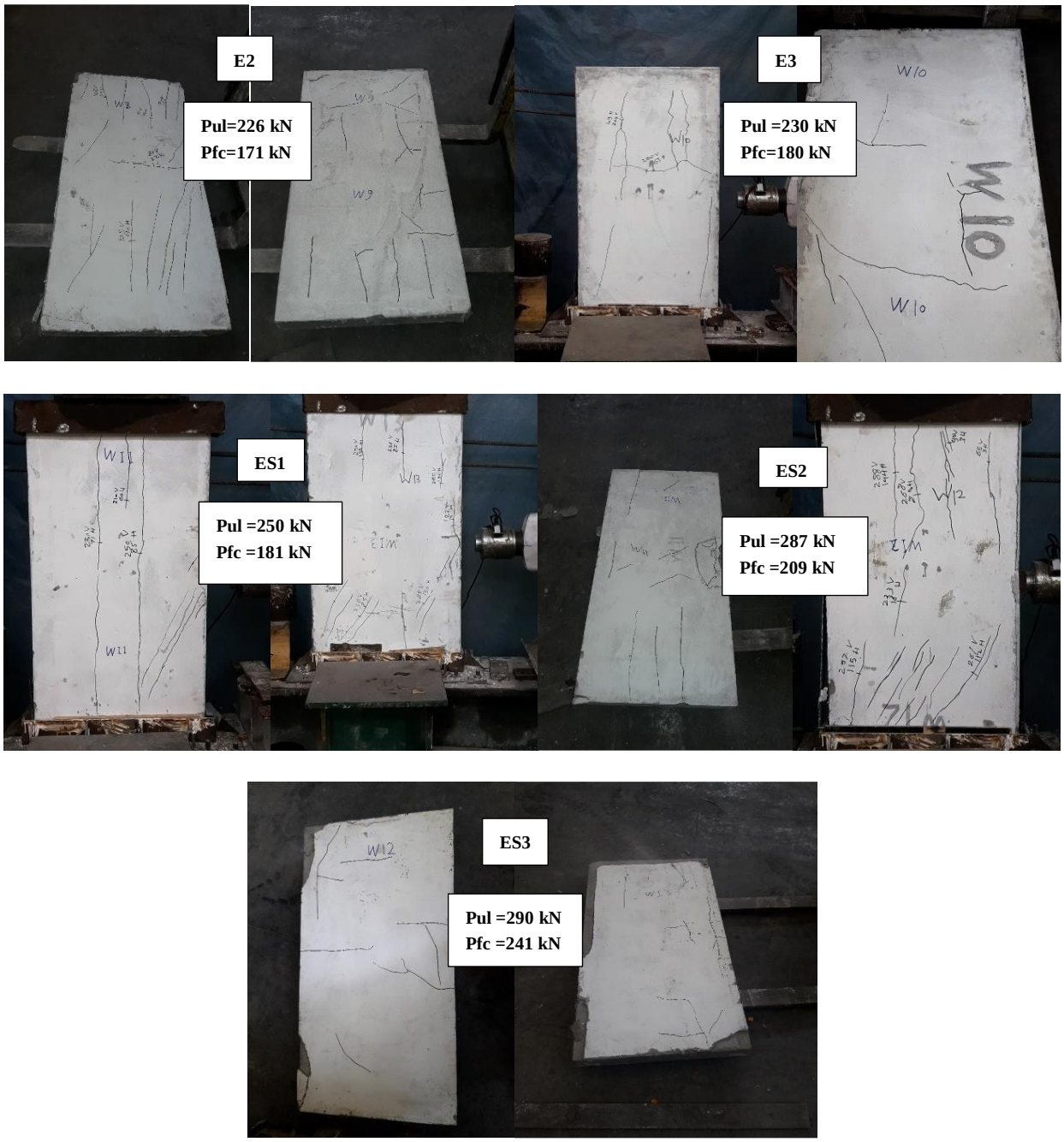

Fig. 27. Crack patterns of the wall.

5.10. Finite element model

A finite element package ABAQUS was used to emulate the performance of ferrocement walls as a nonlinear finite element analysis. This part consist of the initial cracking load, ultimate load, cracking pattern, stress distribution and displacement due to vertical load.

Two kind of elements were used; solid element and truss element. The SOLID 65 (C3D8R) is used to know and emulate the reinforced concrete, truss element (T3D2) is used to know the steel bar by two nodes. Tables 7-9 show the properties of concrete and steel. Fig. 28 displays geometrical model for simulated specimens.

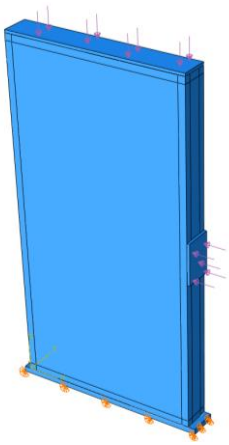

Fig. 28. Geometrical model for simulated specimens.

Table 7. Elastic properties of concrete.

Parameter	Value
Density	2.4×10-9 N/mm³
Mod. of elasticity	21900 MPa
Poisson's ratio	0.168

Table 8. Concrete plasticity parameters.

Parameter	Value
Dilation angle	42
Eccentricity	0.11
f_b/f_c	1.35
K	0.68
Viscosity parameter	0.0001
Yield stress in compression	17 MPa
Cross bonding inelastic strain	0.00
Compressive ultimate stress	33 MPa
Cross bonding inelastic strain	0.00158
Tensile failure stress	3.45 MPa

5.11. Boundary condition

The loads were reacted as pressure on contact area which was (100×650 mm) for compressive load and was (100×100 mm) for side load. The bottom surface of concrete wall was installed to be fixed to prevent from translation XZ, XY, YZ directions and from rotation about XY direction at the two lines of contact with underneath roller supports.

5.12. Finite element results compared with experimental results

The findings of the ferrocement walls were compared with theoretical results and the experimental results. The load-displacement curves for all tested specimens were displayed in figures and have an excellent agreement between theoretical and experimental results as shown in Fig. 29 and Table 10.

Table 9. Elastic properties of steel bars and metal meshes.

Steel 24/35		Welded mesh		Expanded mesh	
Density		Density		Density	
7.86×10-9		7.86×10-9		7.8×10-9	
Mod. of elasticity	Poisson's ratio	Mod. of elasticity	Poisson's ratio	Mod. of elasticity	Poisson's ratio
205000	0.3	170000	0.28	130000	0.28
Stress	Strain	Stress	Strain	Stress	Strain
240	0	413	0.00	199	0
350	0.0951	610	0.05763	320	4.95E-02

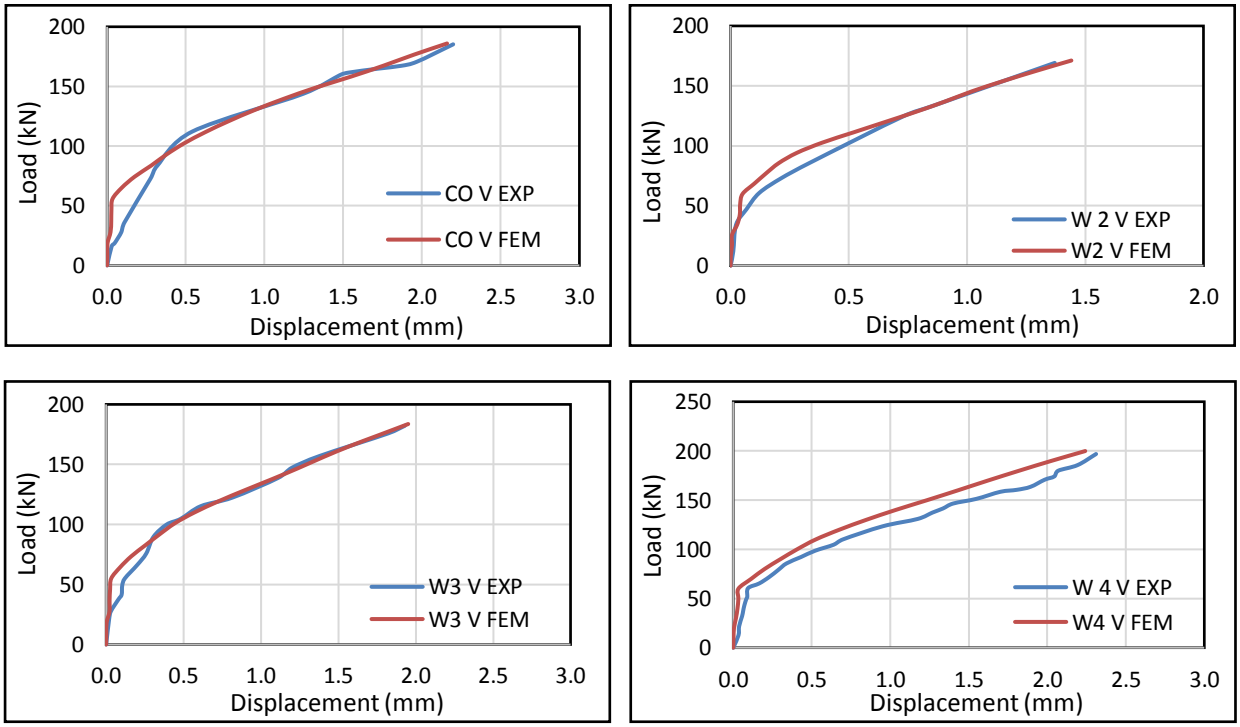

Fig. 29. (continued)

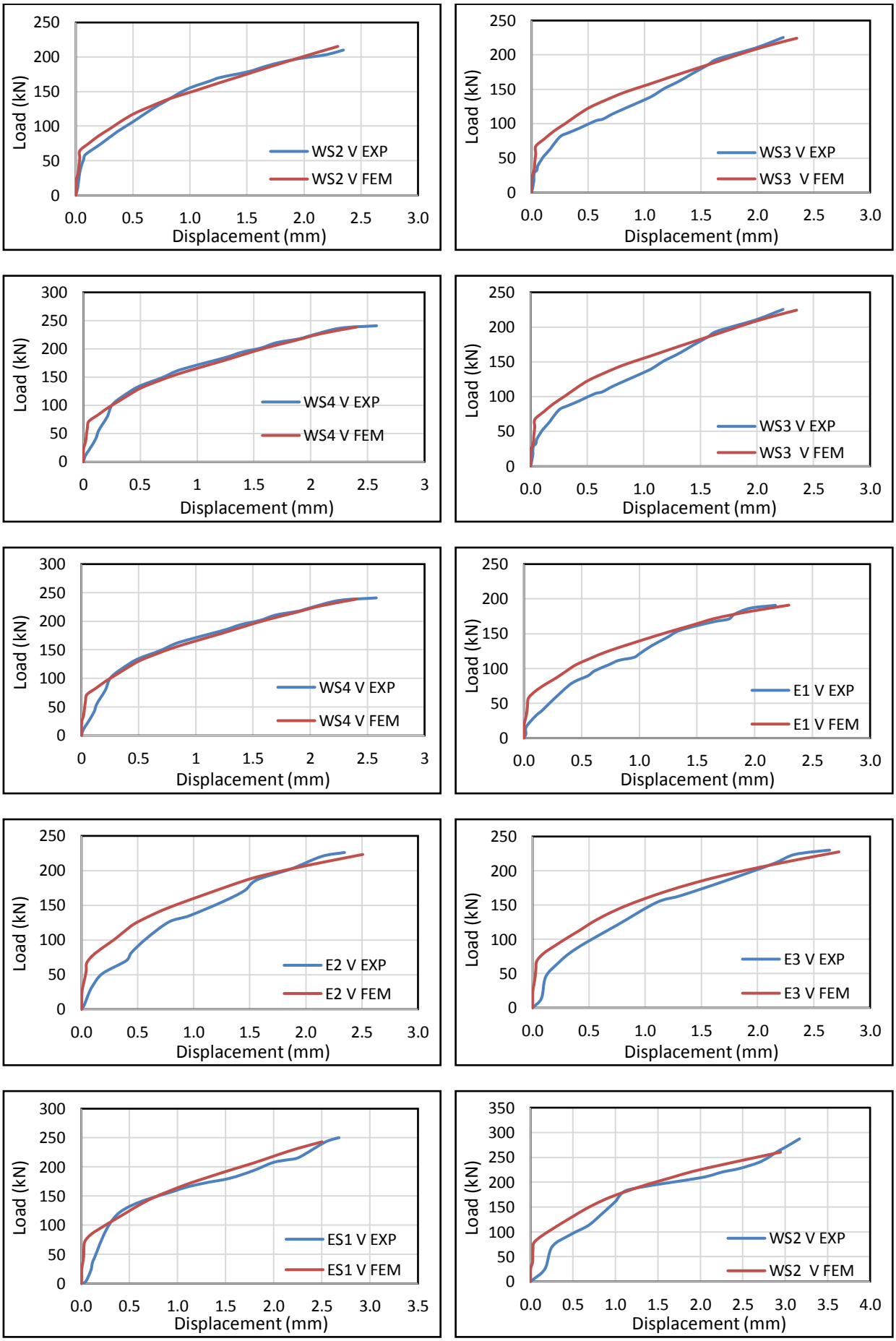

Fig. 29. (continued)

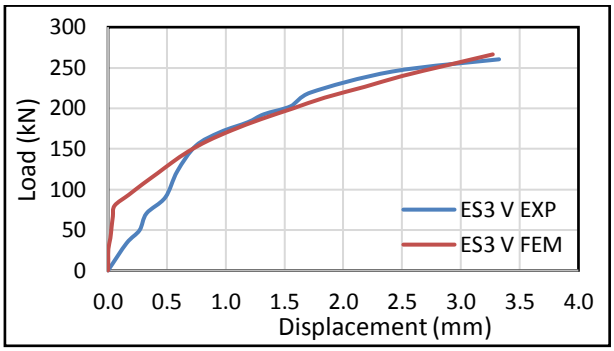

Fig. 29. Comparison between experimental and finite element.

Table 10. Comparison between the results the theoretical and experimental results.

Wall	First crack load (kN)		Ultimate load (kN)		P_{fc} FEM/Exp.	P_{ut} FEM/Exp.
	Exp.	FEM	Exp.	FEM		
CO1	112	148.8	185.3	186.0	1.329	1.004
W2	123	162.6	169.2	171.2	1.322	1.012
W3	133	174.5	182.2	183.6	1.312	1.008
W4	146	179.9	196.9	199.9	1.232	1.015
WS5	161	161.5	210.1	215.4	1.003	1.025
WS3	174	168.2	225.4	224.4	0.967	0.995
WS4	190	179.0	240.8	238.7	0.942	0.991
E1	143	143.3	190.8	191.0	1.002	1.001
E2	171	145.1	226.1	223.2	0.848	0.987
E3	180	159.3	230.2	227.6	0.885	0.989
ES1	181	145.9	250.2	243.1	0.806	0.971
ES2	209	156.23	287.3	260.5	0.748	0.907
ES3	241	159.9	290.4	266.4	0.663	0.918

6. Conclusions

The following conclusions could be formed as follows:

- The ultimate load and rose by 7 and 12% for specimens with three and four layers of steel mesh, respectively, as compared to the wall with two layers of welded steel mesh and energy absorbed increased by 62 and 96%.
- The ultimate load rose by 18 and 21% for specimens with two and three layers of steel mesh, respectively, as compared to the wall with one layer of expanded steel mesh and energy absorbed increased by 22 and 31%.
- Increasing the reinforcing volume percent improved the first fractures, ultimate loads, and energy absorption means increase number of layers meshes reinforcement.
- For the walls reinforced with expanded mesh, the ultimate load was greater than the walls reinforced with welded mesh by 22% and energy absorbed increased by 53%.
- Excellent agreement among theoretical and experimental results.
- Out of this research, using these walls low cost, light weight and can use as precast elements.

It is also suggested to investigate the behavior of the proposed system under impact and dynamic loadings and earth quick load.

Acknowledgements

None declared.

Funding

The authors received no financial support for the research, authorship, and/or publication of this manuscript.

Conflict of Interest

The authors declared no potential conflicts of interest with respect to the research, authorship, and/or publication of this manuscript.

REFERENCES

ACI 213R-87 (1999). Guide for structural lightweight aggregate concrete. ACI manual of concrete practice, American Concrete Institute, Detroit.

ACI 549-R97 (2009). State-of-the-art report on ferrocement. ACI manual of concrete practice, American Concrete Institute, Detroit.

ASTM C494/C494M (2001). Standard specification for chemical admixtures for concrete. ASTM International, West Conshohocken, PA.

ASTM C1116/C1116M-10a (2015). Standard specification for fiber reinforced concrete. ASTM International, West Conshohocken, PA.

Bhalsin S, Shoaib S, Autade P (2014). Tensile strength of ferrocement with respect to specific surface. *International Journal of Innovative Research in Science, Engineering and Technology,* 3(4), 501–507.

E.S.S 4756-11 (2013). Physical and mechanical properties examination of cement, Part 1. Egyptian Standards Specification, Cairo, Egypt.

ECP 203-2007 (2020). Design and construction for reinforced concrete structures. Egyptian Code of Practice: Ministry of Building Construction, Research Center for Housing, Building and Physical Planning, Cairo, Egypt.

Eltehawy E (2009). Effect of using ferro-cement on the mechanical properties of reinforced concrete slabs subjected to dynamic loads. *13th International Conference on Aerospace Science and Aviation Technology.*

Gaba H, Singh H (2008). The study of economy of ferrocement with fly ash as an admixture. *12th International Conference of International Association for Computer Methods and Advances in Geomechanics*.

Naaman AE (2000). Ferrocement and laminated cementitious composites. *Materials and Structures*, 33(1).

Shaheen YB, Eltehawy EA (2017). Structural behavior of ferrocement channels slabs for low cost housing. *Challenge Journal of Concrete Research Letters*, 8(2), 48-64.

Shaheen YBI, Etman ZA, Ramadan AG (2018). Characteristics of ferrocement lightweight wall. *International Journal of Civil Engineering*, 16(1).

Shaheen YBI, Etman ZA, Gomaa O (2019). Structural behavior of thin ferrocement plates with and without stiffeners subjected to compression loading. *Asian Journal of Civil Engineering*, 20, 237–260.

Shaheen YBI, Etman ZA, Marzouk LA (2021). Bending behavior of ferrocement composite semicircular light weight panels for roof construction. *Journal of Materials Science Research and Reviews,* 8(4), 39-71.

Shaheen YBI, Refat HM, Mahmoud AM (2021). Structural behavior of concrete walls reinforced with ferrocement laminates, *Structural Engineering and Mechanics*, 78(4), 455-471.

Shaheen YBI, Etman ZA, Seyam AM (2022). Structural characteristics of lightweight ferrocement walls with various types of core materials and mesh reinforcement. *Current Journal of Applied Science and Technology*, 41(18), 15-45.

Shaheen YBI, Etman ZA, Elhosine NK (2023). Flexural behavior of lightweight ferrocement composite beams. *Advanced Engineering Technology and Application,* 2, 13-23.

Wafa MA, Fukuzawa K (2010). Characteristics of ferrocement thin composite elements using various reinforcement meshes in flexure. *Journal of Reinforced Plastics and Composites,* 29(23), 3530–3539.

Wang S, Naaman AE, Li VC (2004). Bending response of hybrid ferrocement plates with meshes and fibers. *Journal of Ferrocement,* 34(1), 275–288

Challenge Journal of Concrete Research Letters

Research Article

Mechanical, durability and solar reflectance properties of colored self–compacting concrete

Sadık Alper Yıldızel [a,*]

[a] *Department of Civil Engineering, Karamanoğlu Mehmetbey University, 70100 Karaman, Türkiye*

ABSTRACT

Urbanized areas are known to have significantly higher temperatures than rural areas. The Urban Heat Island (UHI) effect is caused by surfaces such as asphalt, buildings, and other heat-absorbing surfaces that store more heat than natural vegetation. Sunlight reflecting properties of building materials are improved with different applications. The present study investigates the mechanical, durability and solar reflectance properties of the colored self-compacting concrete. SCCs containing yellow, green, and black pigments were produced and evaluated. The fresh properties were determined with the slump, L-Box and V-funnel tests. Furthermore, compressive strength, solar reflectance and magnesium sulfate resistance tests were conducted. Yellow pigment added SCC showed a great potential (with the albedo of 0.42) in terms of solar reflectance and decreasing the contribution to the urban heat island effect.

ARTICLE INFO

Article history:
Received 30 May 2023
Revised 17 July 2023
Accepted 26 July 2023

Keywords:
Colored concrete
Pigment
Self-compacting concrete
Urban heat island

1. Introduction

Most people live in urbanized areas, which have a high density of buildings made of concrete or similar construction materials. Concretes produced with gray cement generally have a gray color and, depending on these properties, they absorb a high amount of solar energy and transmit it to the outside as heat (Sanjuán et al. 2022). The heat release mechanism, as is widely well known, has a growing impact on the urban heat island effect (Sen et al. 2022). The most effective way to reduce this effect is to increase the amount of sunlight that is reflected, or to increase the Albedo (Mlilwana and Kearsley 2022; Chen et al. 2019). The albedo of fresh concrete is varied between 0.35 and 0.40, and it decreases to 0.20 as it ages (Kaloush et al. 2008). Many factors, including the ingredients, influence the true albedo of concrete (Sweeney et al. 2011). A previous study conducted by Pomerantz et al. (2003) indicated that the albedo of concrete was generally proportional to the albedo of cement and the albedo of aggregates.

While the availability of local materials restricts the aggregates that can be utilized in concrete production, the most effective way to make concrete more reflective is to replace cement with light-colored cement replacement materials or to use white cement together with color pigments. Boriboonsomsin and Reza studied the effects of the utilization of slag as a cement replacement material on the albedo and it was reported that the albedo of the hardened concrete can be increased by 71 % compared to the reference mixture (Boriboonsomsin and Reza 2007). In another research, Marceau and VanGeem (2008) found that a high albedo can be obtained by coating a concrete surface with photocatalytic agents (Krishnan et al. 2018).

Colored concrete was first used as an aesthetic element in architecture in the United States in the 1980s, when the color, produced by applying iron oxide pigments to the surface or incorporating them into the fresh concrete mixture (Falikman and Deniskin 2021). Colored concrete is now widely used in the production of prefabricated structural elements and non-structural artifacts such as façades and ceilings in all over the world (Hameed and Ali 2021; Junior et al. 2022; Miranda et al. 2019). Self-compacting concrete (SCC) is commonly used for casting these elements, and white cement and

* *Corresponding author*. Tel.: +90-338-226-2000 ; Fax: +90-338-226-2214 ; E-mail address: sayildizel@kmu.edu.tr (S. A. Yıldızel)
ISSN: 2548-0928 / DOI: https://doi.org/10.20528/cjcrl.2023.03.003

color pigments are combined in their manufacture. SCC, as a type of special concrete, can easily slide and flow inside different parts of the formwork due to its own weight, and it does not require vibration (Adhikary et al. 2022). This concrete must be highly flowable and cohesive in order to achieve full compaction (Wani and Ganesh 2022). The cohesiveness and segregation of SCC mixtures can be improved by incorporating viscosity-modifying admixtures (Hameed et al. 2022). Additionally, superplasticizer admixtures can improve the flowability of the mixture (Huang et al. 2018). Since its invention, colored SCC has a wide range of practical applications worldwide. Since the late 1990s, this type of iconic architectural concrete usage has increased dramatically. In addition, the market for colored concrete is anticipated to expand by 6% by 2025(Jesus et al. 2023). However, the major issues with colored concrete are its high production and maintenance costs (López et al. 2016), and it needs optimizing in terms of costs.

This study discusses the advantages of colored SCC. Mechanical, durability and solar reflectance properties of the mixtures were also investigated since there are few studies on this subject in the literature, especially on the self-compacting concrete subject. In addition, in this study, the role of colored concrete in reducing the heat island effect was investigated.

2. Materials and Method

Silica based aggregates were used as both fine and coarse aggregates. CEM II type (42.5R) white cement (WC) conforming to the EN 197(BS EN 197-1 2011) standard was also used. Maximum aggregate size of 20 millimeters was chosen to prevent segregation and its effects. All aggregates are colorless and suitable for painting processes. Density of the coarse and fine aggregates are 2.8 g/cm^3 and 2.5 g/cm^3, respectively. In addition water absorption amounts are 0.4 % and 0.2 % for coarse and fine silica aggregates. Gradation curves of the aggregates and chemical properties of the WC are presented in Fig. 1 and Table 1, respectively. A commercial polycarboxylate based superplasticizer was also utilized. Iron-oxide based three different pigments (green, yellow, black) were also used in the mixtures. The chemical compositions of the pigments are given in Table 2. The mix proportions of the concretes are presented in Table 3. The ingredients were mixed at the rate of 1.27 rad/s for 6 minutes.

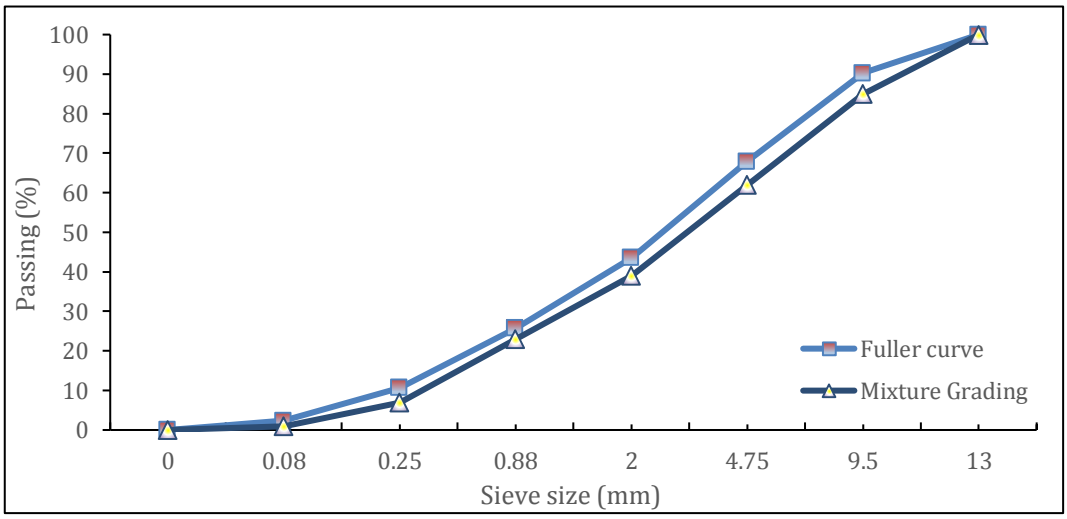

Fig. 1. Aggregate mixture gradation curves.

Table 1. Chemical properties of the white cement (provided by the supplier).

Component	%
Fe_2O_3	3.5
CaO	60.48
Al_2O_3	4.32
MgO	2.37
SiO_2	-
Free CaO	1.69
SO_3	2.61
Na_2O	-
K_2O	-
MnO	-
TiO_2	-

Slump (EN 2009), L-box (CEN 2010) and V funnel (AFNOR 2010) tests were conducted to investigate workability properties of the fresh concrete. Compressive strength tests were performed on the cylindrical (150 x 300 mm) specimens at 3, 7, 28, 60, 90 and 180 days as per the requirements of TS EN 12390-3 (2003).

Table 2. Chemical properties of the pigments (provided by the supplier).

Pigment type	Green	Yellow	Black
$SiO_2 + Al_2O_3$	2.3	1.3	3.1
Fe_2O_3	97	98.9	96.5
Density (g/cm^3)	0.7-0.8	0.4-0.65	0.7-1.1
pH	6-8	3.2-7.3	4-7

Table 3. The mixture proportions.

Sample	WC (kg/m³)	Silica agg.-Coarse (kg/m³)	Silica sand-Fine (kg/m³)	Water/Binder	Pigment type	Pigment amount (by the w. of WC%)	Superpl. (by the w. of C%)
Ref.	400	850	750	0.43	-	-	1.5
SCC-G_1	400	850	750	0.43	Green	2.5	1.5
SCC-G_2	400	850	750	0.43	Green	5.0	1.5
SCC-G_3	400	850	750	0.43	Green	7.5	1.5
SCC-Y_1	400	850	750	0.43	Yellow	2.5	1.5
SCC-Y_2	400	850	750	0.43	Yellow	5.0	1.5
SCC-Y_3	400	850	750	0.43	Yellow	7.5	1.5
SCC-B_1	400	850	750	0.43	Black	2.5	1.5
SCC-B_2	400	850	750	0.43	Black	5.0	1.5
SCC-B_3	400	850	750	0.43	Black	7.5	1.5

Sulfate attack on concrete specimens were also investigated in terms of compressive strength losses at 3, 7, 28, 60, 90 and 180 days. During the sulfate attack tests, two groups of samples were prepared. One group was kept in curing water, while the other was kept in a solution containing 10 percent magnesium sulfate. The concentration of magnesium sulfate was refreshed every 20 days until the end of the test period. Albedo values of the specimens were measured with an UV-VIS-NIR spectrophotometer (Fig. 2). In addition, rectangular specimens (24x24x5 mm) were prepared for the measurement (Fig. 3). Albedo properties were determined by examining wavelengths between 200 and 2500 nm. Mean percentages of reflections were measured, and albedo values for each sample were determined based on spectrophotometer readings.

In the first step of the experimental studies, the albedo value of the specimens was measured after 28 days of curing. The average of three measurements of the spectral reflectance of each specimen was recorded.

Fig. 2. UV-VIS-NIR spectrophotometer.

Fig. 3. Albedo test samples.

3. Results and Discussion

The albedo values of the samples are given in Fig. 4. The test results range from 0.29 to 0.42. SCC-Y3 had the highest albedo, but SCC-test B3's result was the lowest, as expected (Kaloush et al. 2008). Albedos decreased as black pigment content increased.

Slump, L-box and V-funnel test results are shown in Figs. 5-7 respectively. Workability of the samples decreased on the inclusion of pigments. The value of slump flow varied between 712 and 725 mm for all mixtures conforming to the limits of EFNARC ((category of SF2) EFNARC 2002). The filling ability of the pigment added mixtures decreased due to the high-water absorption characteristics of pigments. In accordance with the present results, previous studies have demonstrated that pigment inclusion increases water demand of the concrete mixtures (Jesus et al. 2023; Hunek and Szafraniec 2021; Ghadban and Abdulrehman 2022).

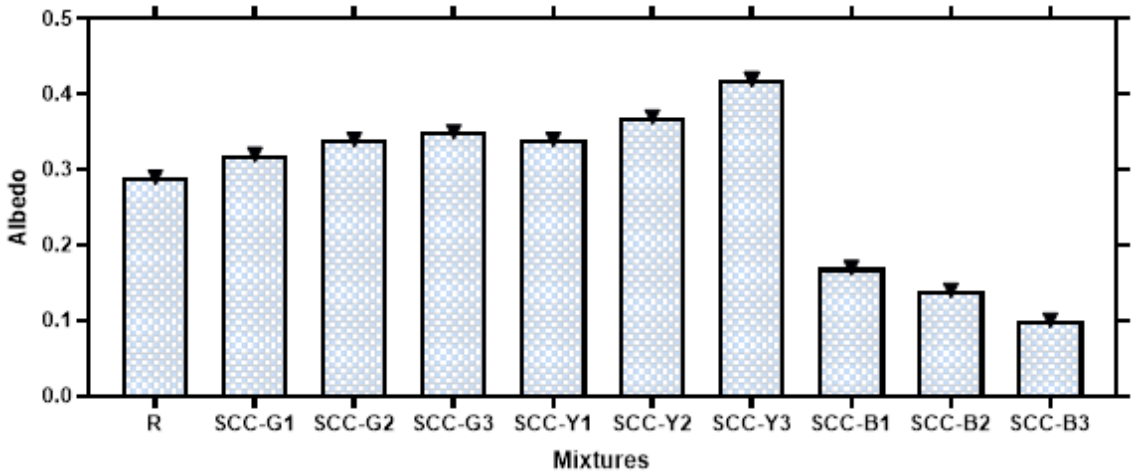

Fig. 4. Albedo of test samples.

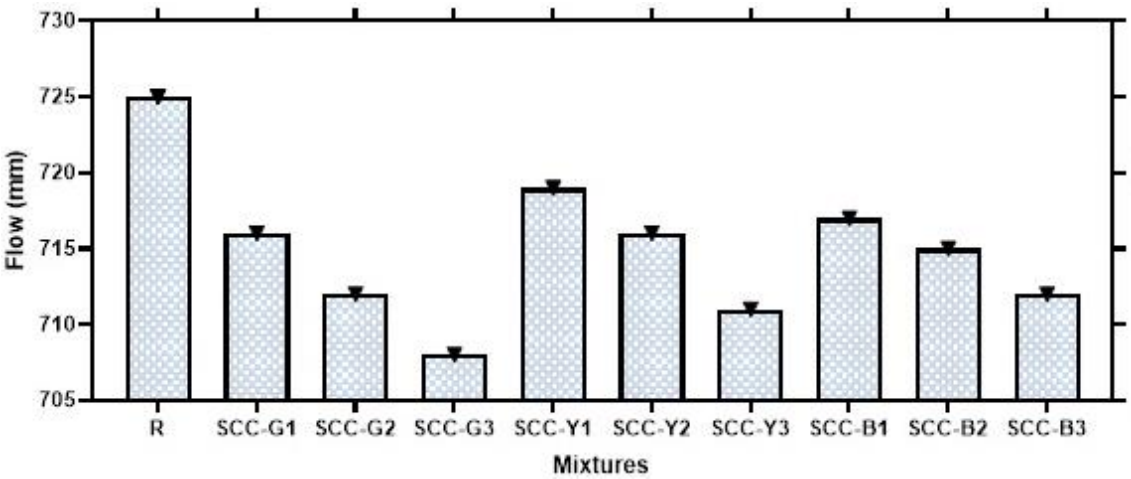

Fig. 5. Slump test results.

It was obtained that V-funnel times varied between 14 and 25 sec. (Fig. 7) and all samples were in the class of VS2 according to the ENFARC on the basis of viscosity (EFNARC 2002). In Fig. 6, there is a clear trend of increasing blocking ratios varied from 0.81 to 0.91 for all mixtures. The blocking ratios of the mixtures were classified as PA2. The blocking ratios of the mixtures were classified as PA2. These results are in parallel with similar studies (Hunek and Szafraniec 2021; Ghadban and Abdulrehman 2022).

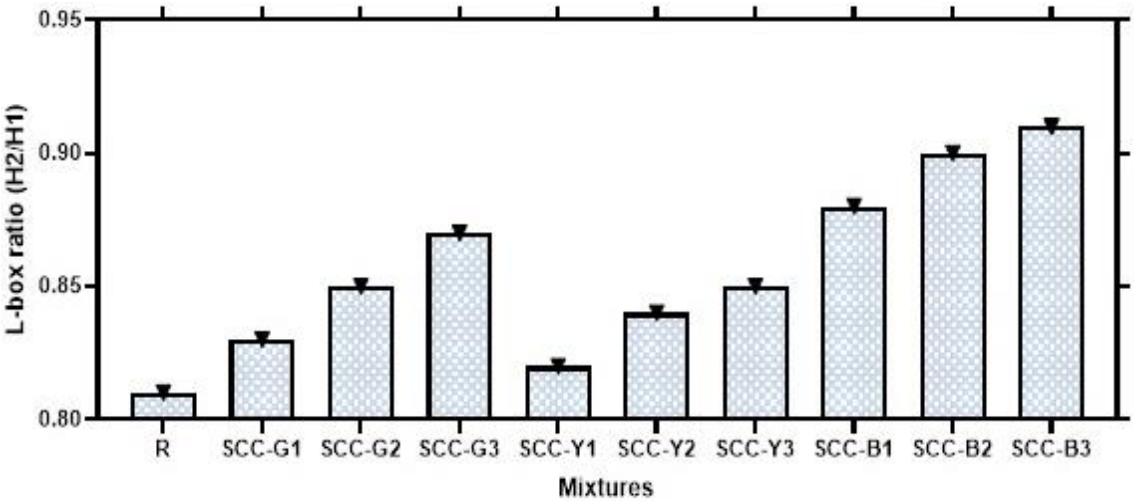

Fig. 6. L-box test results.

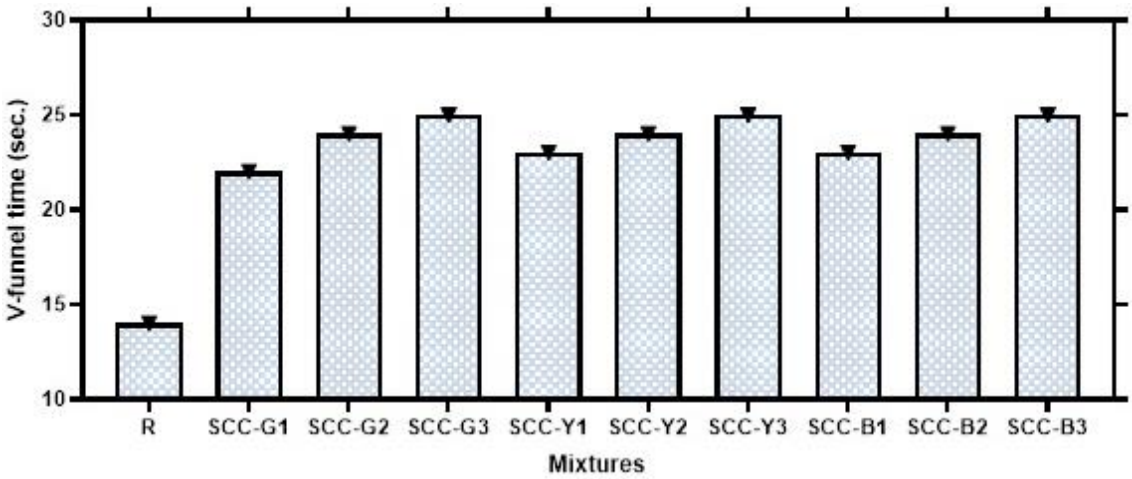

Fig. 7. V-funnel time.

Compressive strength test results at 7, 28, 60, 90 and 180 days are presented in Fig. 8. Compressive strengths increased for all samples with the increasing curing time (Kovačević et al. 2021; Akinpelu et al. 2019). Moreover, the pigment inclusion had very limited effect on the compressive strengths since all mixture had the cement and water to binder contents (Hoang et al. 2022; Djamila and Mohamed 2018).

The resistance of specimens to magnesium sulfate decreased with exposure time, as shown in Fig. 9. The most deleterious effect was obtained for the SCC-B3 mixture at 180 days and, compressive strength losses increased for all samples depending on the exposure time. These results are also compatible with the literature results (Zhao et al. 2019; Yang et al. 2023; Mostofinejad et al. 2020).

4. Conclusions

In this study, some mechanical, durability and solar reflectance properties of colored self-compacting concrete were investigated. Based on the experimental test results, following results can be drawn:

- SCC-Y3 sample showed the highest albedo, and black pigment added samples reflected the lowest albedo results as expected.
- Due to the high-water absorption characteristics of pigments, the filling ability of the pigment-added mixtures decreased. Moreover, the addition of pigment increased the water demand of concrete mixtures.
- The pigment inclusion had a negligible effect on the compressive strengths, as all mixtures contained the same proportions of cement and water to binder.
- The magnesium sulfate resistance of all samples decreased with the increasing time.

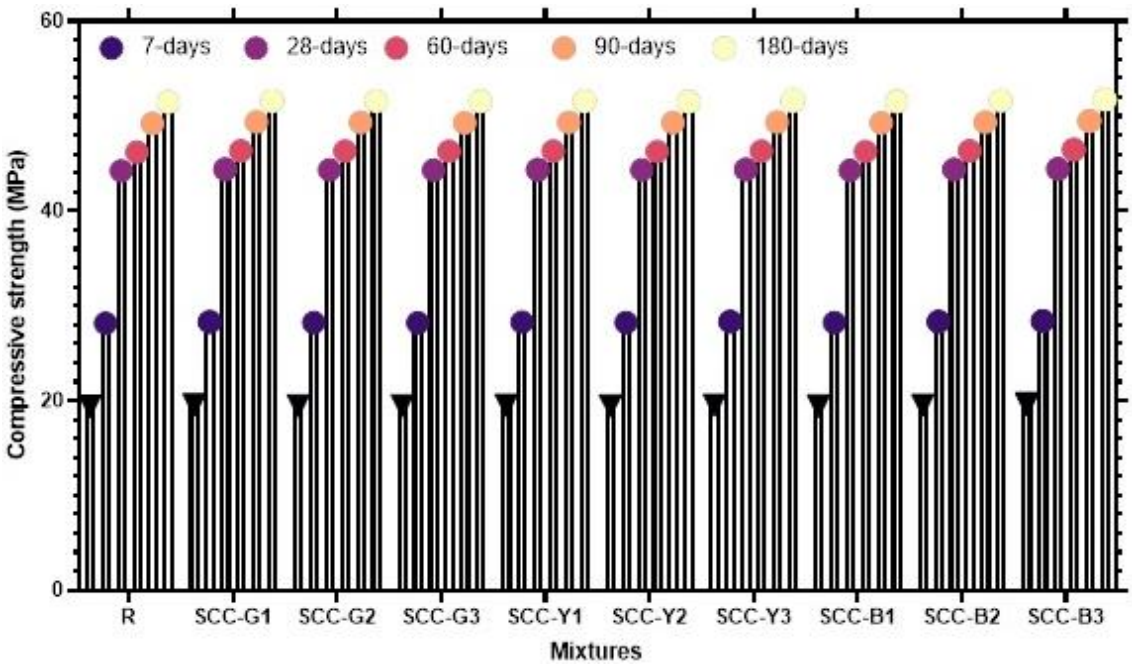

Fig. 8. Compressive strength test results.

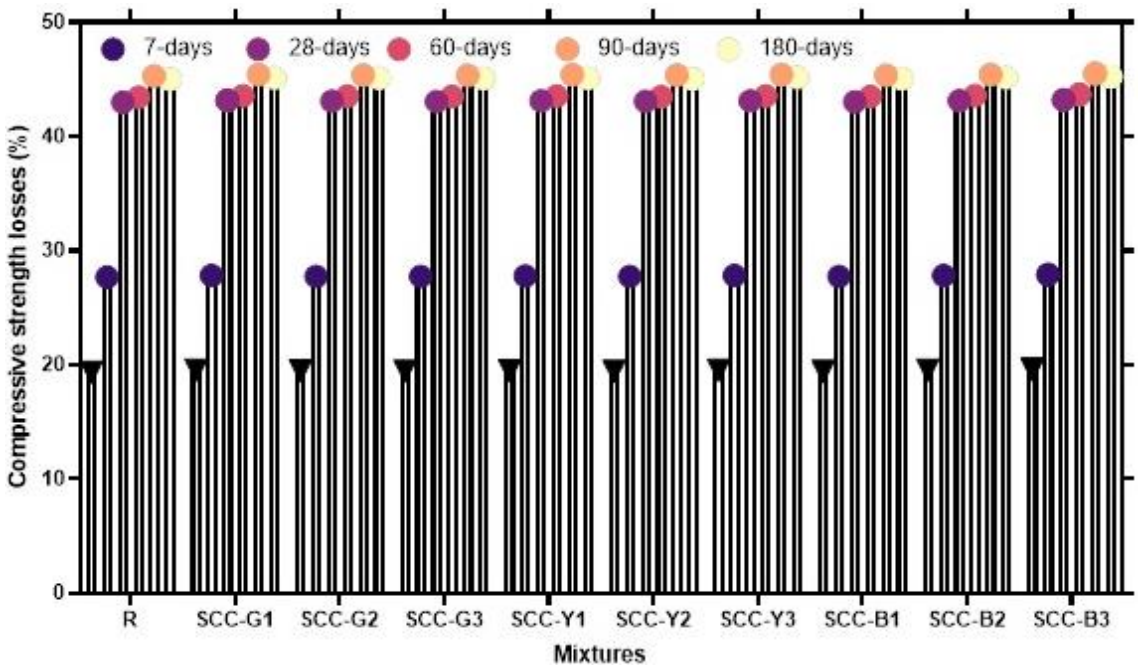

Fig. 9. Compressive strength losses (%).

Acknowledgements

This research has been carried out with the support of Karamanoğlu Mehmetbey University Scientific Research Projects Coordinatorship under Project Number of 14-M-21. The authors would like to thank Karamanoğlu Mehmetbey University for their support.

Funding

The author received no financial support for the research, authorship, and/or publication of this manuscript.

Conflict of Interest

The author declared no potential conflicts of interest with respect to the research, authorship, and/or publication of this manuscript.

References

Ahmad WT, Ganesh S (2022). Study on fresh properties, mechanical properties and microstructure behavior of fiber reinforced self-compacting concrete: A review. *Materials Today Proceeding*, 62.

Adhikary SK, Ashish DK, Sharma H, Patel J, Rudžionis Ž, Al-Ajamee M, Thomas BS, Khatib JM (2022). Lightweight self-compacting concrete: A review. *Resources, Conservation & Recycling Advances*, 15.

AFNOR (2010). NF EN 12350-9: Testing fresh concrete - Part 9: Self-compacting concrete - V-funnel test, European standard, EU.

Akinpelu MA, Odeyemi SO, Olafusi OS, Muhammed F (2019). Evaluation of splitting tensile and compressive strength relationship of self-compacting concrete, *Journal of King Saud University - Engineering Sciences*, 31.

Barnat-Hunek D, Szafraniec M (2021). Influence of biodegradable release oils on the physical and mechanical properties of light-colored architectural concrete, *Materials (Basel)*, 14.

Boriboonsomsin K, Reza F (2007). Mix design and benefit evaluation of high solar reflectance concrete for pavements. *Transportation Research Record: Journal of the Transportation Research Board*, 2011(1).

CEN (2010). CYS EN 12350-10:2010 Testing fresh concrete, Part 10: Self-compacting concrete -L box test. Cyprus, EU.

Chen J, Chu R, Wang H, Zhang L, Chen X, Du Y (2019). Alleviating urban heat island effect using high-conductivity permeable concrete pavement. *Journal of Cleaner Production*, 237.

Djamila B, Mohamed G (2018). The use of non-destructive tests to estimate Self-compacting concrete compressive strength. *MATEC Web of Conferences,* Oradea, Romania.

EFNARC (2002). Specification and Guidelines for Self-Compacting Concrete, EU.

EN 197-1 (2011). Cement Composition, specifications and conformity criteria for common cements. European Standard, EU.

EN 12350-2 (2009). Testing fresh concrete – Part 2: Slump test. European Standard, EU.

Falikman VR, Deniskin VV (2021). Architectural Concrete versus White Stone: A New Approach to Restoring Historical Heritage. *RILEM Book Series*, Belgium.

Ghadban RA, Abdulrehman MA (2022). Study of some properties of colored geopolymer concrete consisting of slag. *Journal of the Mechanical Behavior of Materials*, 31(1).

Hameed A, Rasool AM, Ibrahim YE, Afzal MFUD, Qazi AU, Hameed I (2022). Utilization of fly ash as a viscosity-modifying agent to produce cost-effective, self-compacting concrete: A sustainable solution. *Sustainability,* 14.

Hameed MM, Ali AM (2021). Using of metakaolin to produce colored geopolymer concrete. *Journal of Physics: Conference Series*, İstanbul, Turkey.

Hoang ND (2022). Machine Learning-Based Estimation of the Compressive Strength of Self-Compacting Concrete: A Multi-Dataset Study. *Mathematics,* 10.

Huang F, Li H, Yi Z, Wang Z, Xie Y (2018). The rheological properties of self-compacting concrete containing superplasticizer and air-entraining agent. *Construction and Building Materials*, 166.

Jesus CF, Arruda Junior ES, Braga NTS, Silva Junior JA, Barata MS (2023). Coloured concrete produced from low-carbon cements: Mechanical

properties, chromatic stability and sustainability. *Journal of Building Engineering*, 67.

Junior ESA, Barata MS, Secco P, Carvalho ES (2022). The use of red mud and kaolin waste in the production of a new building material: Pozzolanic pigment for colored concrete and mortar. Revista Materia, 27.

Kaloush KE, Carlson JD, Golden JS, Phelan PE (2008). The Thermal and radiative characteristics of concrete pavements in mitigating urban heat island effects. *Portland Cement Association*, Illionis, USA.

Kovačević M, Lozančić S, Nyarko EK, Hadzima M (2021). Modeling of compressive strength of self-compacting rubberized concrete using machine learning. *Materials (Basel)*, 14.

López A, Guzmán GA, Di Sarli AR (2016). Color stability in mortars and concretes, Part 2: Study on architectural concretes. *Construction and Building Materials*, 123.

Marceau ML, VanGeem MG (2008). Solar reflectance values for concrete. *Concrete International*, 30(8), 52-58.

Mlilwana TP, Kearsley EP (2022). Light-coloured concrete surfacing for urban heat-island mitigation in Southern Africa. *Journal of South African Institution of Civil Engineering*, 64.

Miranda J, Valença J, Júlio E (2019). Colored concrete restoration method: For chromatic design and application of restoration mortars on smooth surfaces of colored concrete. *Structural Concrete*, 20.

Mostofinejad D, Hosseini SM, Nosouhian F, Ozbakkaloglu T, Nader Tehrani B (2020). Durability of concrete containing recycled concrete coarse and fine aggregates and milled waste glass in magnesium sulfate environment. *Journal of Building Engine*ering, 29.

Pomerantz M, Akbari H, Chang S C, Levinson R, Pon B (2003). Examples of Cooler Reflective Streets for Urban Heat-Island Mitigation : Portland Cement Concrete and Chip Seals. Lawrence Berkeley National Lab., USA.

Sanjuán MÁ, Morales Á, Zaragoza A (2022). Precast Concrete Pavements of High Albedo to Achieve the Net "Zero-Emissions" Commitments. *Applied Science*, 12.

Sen S, Li H, Khazanovich L (2022). Effect of climate change and urban heat islands on the deterioration of concrete roads. *Results in Engineering*, 16.

Sweeney M, Spinazzola R, Morrison D, Macklin D, Marion J (2011). Advanced manufacturing technologies for reduced cost and weight in portable ruggedized VIS-IR and multi-mode optical systems for land, sea, and air. *Proceedings Volume 8012, Infrared Technology and Applications XXXVII*.

TS EN 12390-3 (2003). Testing hardened concrete-Part 3: Compressive strength of test specimens. Ankara, Turkiye.

Wu Y, Krishnan P, Zhang MH, Yu LE (2018). Using photocatalytic coating to maintain solar reflectance and lower cooling energy consumption of buildings. *Energy and Buildings*, 164.

Yang Y, Kang Z, Zhan B, Gao P, Yu Q, Xiong Y, Wang J, Zhang Y (2023). Durability of green concrete in severe environment. *Journal of Renewable Materials*, 11.

Zhao G, Li J, Han F, Shi M, Fan H (2019). Sulfate-induced degradation of cast-in-situ concrete influenced by magnesium. *Construction and Building Materials*, 199.